ResearchGate

See discussions, stats, and author profiles for this publication at: https://www.researchgate.net/publication/318681609

Selenium, tellurium and sulfur variations in basalts along the Reykjanes Ridge and extension over Iceland, from 50°N to 65°N

Working Paper · July 2017

DOI: 10.1594/IEDA/100700

CITATIONS
0

READS
3

3 authors, including:

Katherine Kelley
University of Rhode Island

133 PUBLICATIONS **2,477** CITATIONS

SEE PROFILE

All content following this page was uploaded by Katherine Kelley on 25 July 2017.

The user has requested enhancement of the downloaded file.

Selenium, tellurium and sulfur variations in basalts along the Reykjanes Ridge and extension over Iceland, from 50°N to 65°N

Allison Forrest, *Graduate School of Oceanography, University of Rhode Island, Narragansett, RI, 02882, USA (lucky66@gmail.com)*

Katherine A. Kelley*, *Graduate School of Oceanography, University of Rhode Island, Narragansett, RI, 02882, USA*
(kelley@uri.edu)

Jean-Guy Schilling*, *Graduate School of Oceanography, University of Rhode Island, Narragansett, RI, 02882, USA (jgs@gso.uri.edu)*

**Corresponding Authors*

Unpublished manuscript posted 25 July 2017, and accompanying the published data set:
Forrest, Allison, et al., (2017), S, Se and Te contents of basalts from the Reykjanes Ridge and SW Iceland Rift Zone. Interdisciplinary Earth Data Alliance (IEDA). doi:10.1594/IEDA/100700

Abstract.

We report on the S, Se, and Te contents of basalts from the well-documented Reykjanes Ridge and extension over the SW-Iceland rift zone, along where the Iceland mantle plume appears to have dispersed and mixed with the surrounding depleted upper mantle. Most of the submarine basalts are from glassy rims, including 5 sub-glacial erupted Iceland basalts. We emphasize that our interpretation of these data is based primarily on the along-ridge spatial variations, considering that the nature of the large-scale sampling and sampling-intervals involved preclude determining local consanguineous basaltic melt evolutions.

Sulfur variation along the ridge stays fairly constant (1000-1500 ppm range), until it drops drastically around 63°N coincident with the onset of degassing of H_2O. Chlorine and bromine degassing also take place at shallow water depths of 250-500 m. The S variation is clearly controlled by its solubility, by sulfide-saturation from 50°N to 63°N, and as vapor/melt solubility further north and on Iceland. In contrast, Se and Te increase regularly from 50°N toward Iceland by a factor of 2-2.5 and 4-5, respectively, until degassing of S and other volatiles takes place. About 95% of S, 80% of Te and 67% of Se are lost by degassing north of 63°N. The increase in Se and Te from 50-63°N is clearly unrelated to low pressure, late stage, crystallization variation, as evident by the accompanying along-ridge variations in MgO, Ni and Cu from the same basalts.

Two models might account for the Se and Te enrichments of the undegassed basalts. First, these variations could result from along-ridge dilution of the Iceland mantle plume, presumably enriched in Se and Te and Te/Se ratio relative to the depleted upper mantle (DUM), as previously inferred from Pb-Sr-Nd and He isotope variations of the same basalts. The positive correlations of Se, Te and Te/Se ratio of the undegassed MORB population with $^3He/^4He$, as well as Cu with $^3He/^4He$ from 50°N-65°N, are both supportive of this explanation. Alternatively, increasing melting toward Iceland of a single sulfide-bearing primary upper mantle source (PUM) with BSE composition (i.e., 250 ppm S [714 ppm sulfide], 75 ppb Se and 12 ppb Te) can also broadly match the observed trends of increasing Se and Te and Te/Se ratio toward Iceland, providing the following conditions apply: 1) the degree of partial melting from 50-65°N increases from 7-19%, and 2) the Se and Te sulfide melt/silicate melt partition coefficients are in

the range of 10^3 for Se and 10^4 for Te for basalts ranging between 9-7 % MgO. These two models are not mutually exclusive, and both are likely. The extent to which each process dominates the observed Se, Te, and Cu variations remains uncertain in light of the inherent uncertainties in the involved model parameters.

Finally, we note that the distinctly longer scale-length of the mixing gradients observed for Se, Te, Se/Te, Cu, PGE and $^3He/^4He$, and the thermally related elevation of the ridge axis, compared to the shorter scale-length of the mixing gradients previously established for Nd-Sr-Hf-Pb isotopes and other refractory trace elements along the Reykjanes Ridge, remain poorly understood and the possible cause(s) speculative, warranting further exploration.

1. Introduction.

Under high-temperature, sulfide-saturated mantle and magmatic conditions, the geochemical behaviors of the related chalcophile and volatile trace elements Se and Te are likely to be dominantly controlled by the presence of sulfides and their ability to substitute for S. This is in part evident from 1) the presence of Se and Te in magmatic sulfide ores (e.g., Barnes et al., 2009; Eckstrand et al., 1989; Greenland and Campbell, 1977) and meteorites (e.g., Dreibus et al., 1995; DuFresne, 1960), 2) early experimental sulfide phase determinations showing complete liquid solutions in the S-Se, S-Te, and Se-Te binary systems (Kullerud, 1970), and more recently 3) in-situ analyses of sulfides in peridotites and their whole-rock budgets (e.g., Guo et al., 1999; Hattori et al., 2002; König et al., 2015; Lorand and Alard, 2010). Yet, because of the extremely low abundance of Se and Te in the earth, very little is known about their abundances and variations during processes of basalt formation and evolution, including sulfide/silicate melt partitioning.

Estimates of S, Se, and Te in the bulk silicate earth (BSE) consider them to be depleted by 3 orders of magnitude relative to CI carbonaceous chondrites (McDonough and Sun, 1995). These very low abundances are usually attributed to 1) the very high volatility of Se and Te, and to a lesser extent S, during condensation of the solar system, 2) the sequestration of S, Se, and Te (and highly siderophile elements [HSE]) into the Fe-rich core during its formation, and 3) their compensation by an addition of a CI chondrite veneer rich in HSEs and volatiles, including S,

Se, and Te, during the late-stage accretion of the earth (e.g., McDonough and Sun, 1995; O'Neill and Palme, 1998; Wang and Becker, 2013). Based on the study of a small number of peridotitic rocks, the relative abundances of S, Se, and Te are also believed to be essentially chondritic, as are the platinum group elements (PGE; Lorand and Alard, 2010; Morgan, 1986), although data from ultra-depleted orogenic peridotites cast some uncertainty on this assertion (König et al., 2012).

As a result of such low abundances and analytical detection limitations, very little is known about Se and Te in ocean island and mid-ocean ridge basalts and their fractionation relative to S during either partial melting of various sulfide-bearing mantle sources (including sulfide-melt production), followed possibly by sulfide precipitation during magma ascent and fractional crystallization, or during relative degassing during volcanic eruptions, sub-aerially or at low submarine water depth and hydrostatic pressure, in addition to possible Se and Te mantle source heterogeneities. In order to provide additional constraints on some of these questions, we now report the Se, Te and S contents of 94 basalts from the Reykjanes Ridge and its extension on the SW Iceland rift zone, from 50 to 65°N (Fig. 1), using a new hydride generation-inductively coupled plasma-mass spectrometry (HG-ICP-MS) analytical method we have developed (Forrest et al., 2009). Numerous isotopic, trace element and petrologic studies of these very same basalts have shown that this region of the Mid-Atlantic Ridge is the locus of a dynamical mixing interaction and dilution of the Iceland mantle plume with DUM (e.g., Fig.2; Blichert-Toft et al., 2005; Hart et al., 1973; Poreda et al., 1986; Schilling, 1973; Schilling et al., 1983; Sun et al., 1975). The progressive rise of the ridge axis from 4 km water depth to 0.4 km above sea level (Fig. 2), and sub-glacial eruptions, also provide a natural laboratory to study the effect of hydrostatic pressure on eruptive degassing of S, Se and Te relative to other volatiles, such as the halogens (Rowe and Schilling, 1979; Unni and Schilling, 1978), and water (Moore and Schilling, 1973; Nichols et al., 2002; Poreda et al., 1986).

2. Samples.

The petrologic characteristics of these basalts have been studied in detail. They are all olivine to slightly quartz normative tholeiitic basalts, except for one strongly light-rare earth (REE) depleted sub-glacial erupted glassy picrite (Ic117g). Whole-rock major, REE and other trace element contents, as well as phenocryst modal abundances, and their petrographic assemblages (including % vesicles), can be found in Schilling et al. (1983), and Moore and Schilling (1973). Major elements of the glass rims of these MORB and the sub-glacial Iceland basalts can be found in Sigurdsson (1981), and 40 trace elements from the Reykjanes Ridge basalt glasses in Kelley et al. (2013).

Noteworthy for interpretation is the pronounced minimum in Mg-value (i.e., molar Mg/[Mg+Fe]; or MgO) and Ni content observed around 63.5°N, although a similar minimum for Cu is absent (Fig. 3). This minimum also corresponds to a minimum in the temperature of crystallization of olivine micro-phenocrysts present in these basalts, as determined from the Fe and Mg olivine crystal/melt (glass) partitioning (Hermes and Schilling, 1976; Schilling and Sigurdsson, 1979). This temperature minimum has also been confirmed by one atmosphere melting and re-crystallization experiments of 16 of these basalts (Fisk, 1978; Fisk et al., 1980). The sequence of crystallization of olivine, plagioclase and clinopyroxene in these melting experiments also suggests that prior to eruption these basalts may have suffered some crystallization within a pressure range of 2 to 6.2 kb (0.2-0.62 GPa), with a 2 kb minimum around 63°N, which also coincides with the temperature minimum and maximum extent of crystallization observed along the Reykjanes Ridge. The more extensive low-P crystallization in this region coincides with the thicker crust of the Iceland shelf margin and the small en-echelon shifts of the ridge axis as it approaches the leaky transform fault zone present over the Reykjanes Peninsula and eastward.

3. Analytical Methods.

3.1 Selenium and Tellurium.

The selenium and tellurium contents of the basalts were determined by HG-ICP-MS. Details of the method, precision and accuracy are reported in Forrest (2005) and Forrest et al.

(2009). The Se and Te reported here were obtained at the same time as this method was developed. Analytical precision is 12.2 to 15.1% for Se and 4.6 to 7.2% for Te, based on repeated measurements of Se and Te concentrations in an in-house Mid-Ocean Ridge basalt standard EN026 10D-3 (Mohns Ridge basalt) and in USGS standard BHVO-2 (Hawaiian basalt). This technique recovers recommended concentrations of Se in the reference materials used for calibration within 14 ppb (see Figure S1 of the supplement and Forrest et al. (2009)).

3.2 Sulfur.

The sulfur contents of the basalt glasses were determined with a five-spectrometer Cameca SX-100 electron microprobe at the American Museum of Natural History, NY. Sulfur analyses were done in trace mode with a 15 kV accelerating voltage, 40 nanoamp beam current, and 20-micron diameter beam utilizing a wavelength-dispersive spectrometer equipped with a large PET (LPET) diffracting crystal. Count time on the sulfur K-alpha peak was 220 seconds and count time on background was 40 seconds. Staunton troilite (FeS) was used for sulfur X-ray calibration based on results from several sulfur K-alpha wavelength scans done on a few glass chips in each probe mount to determine the appropriate sulfur calibration standard (C. Mandeville, personal communication).

Basalts devoid of glass, sub-aerially or submarine erupted, were crushed into powder for sulfur analysis by X-Ray Fluorescence (XRF) spectroscopy, using a routine method for lunar and terrestrial basalts developed By M. Rhodes from the University of Massachusetts, Amherst . The powdered samples were pressed into pellets and analyzed for sulfur by XRF using a Phillips PW 2400 X-ray spectrograph with Rh-tube operated at 30 kV and 100 mA, and a Ge crystal and flow detector at the University of Massachusetts, Amherst. The XRF method was calibrated using MAG-1 marine sediment from the USGS (S = 3900 ppm), and the Allende meterorite (S = 2.1 wt. %), and the matrix corrections were done using the major element contents of these basalts (Schilling et al., 1983; Sigurdsson, 1981). The detection limit for the sulfur analysis by this standard XRF method is 3–5 ppm .

4. Results.

Table 1 lists the S, Se and Te contents of 108 basalts, as well as the corresponding Cu contents and $(La/Sm)_N$ ratios for the Reykjanes ridge (Kelley et al., 2013) and Iceland (Schilling et al., 1983 and unpublished), and the volume % of vesicles (Moore and Schilling, 1973; Schilling et al., 1983). The table includes 58 glasses from the Reykjanes Ridge and 5 glasses from sub-glacially erupted Iceland basalts. The other 17 Iceland basalts are from sub-aerial flows. Along the Reykjanes Ridge, whole–rock basalt analyses are either from basalts devoid of glass, erupted at water depths less than 162 m close to Iceland (n=5 basalts), or from the interiors of pillow basalts from dredge stations with or without glass available. A comparison of S, Se and Te basalt contents between glass and pillow interiors from this data set is discussed in Forrest (2005), and briefly below in Section 6.

Except for water depths shallower than ~500 m near Iceland, where degassing of volatiles such as S, H_2O, Cl and Br has previously been observed (Moore and Schilling, 1973; Moore and Calk, 1991; Nichols et al., 2002; Unni and Schilling, 1978), the sulfur content of basalts in this study varies between 970 and 1790 ppm, which is within the range observed in many sulfide-saturated MORB (e.g., Czamanske and Moore, 1977; Mathez, 1976; and references therein). Selenium contents of these undegassed Reykjanes Ridge basalts varies between 84 and 328 ppb, which is similar to the Se range found for a very few other N-MORB previously reported from the Atlantic and other oceans (Hertogen et al., 1980; Laul et al., 1972; Yi et al., 2000), and larger than the 124-204 ppb range of N-,T- and LOMU- MORB from the 45°S-50°S MAR reported by Lissner et al. (2014). In contrast to these studies and ours, the Se concentrations of the N-MORB glasses reported by Jenner and O'Neill (2012) appear systematically higher, up to a factor of 2-3, which may reflect an analytical bias (See Supplement Figure S1, along with related discussion on sulfide globule/silicate melt partition coefficients for Se measured in MORB by Patten et al. (2013)). The Te contents of undegassed samples range from 2 to 16 ppb, a significantly larger variation than the 1.2 to 5 ppm range seen for typical N-MORB in previous studies (Hertogen et al., 1980; Yi et al., 2000), and the 2-9.5 ppb range of N-MORB, T-MORB and LOMU-MORB from the 45°S-50°S MAR reported by Lissner et al. (2014). The 5 sub-glacial erupted Iceland basalt glasses range from 109-177 ppb in Se, 5.9-15 ppb in Te, and 480-715 ppm in S.

5. Spatial variations in S, Se, and Te.

5.1 Sulfur.

The latitudinal sulfur variation stays fairly constant, mostly in the range of 1000-1500 ppm (Fig. 4a), until it drops drastically where degassing of Cl, Br, and H_2O in the same samples is observed around 63°N, at a water depth of 250-500 meters (Fig. 2; Moore and Schilling, 1973; Nichols et al., 2002; Unni and Schilling, 1978). The drop in S and other volatiles also coincides with a maximum in the vesicle volume % present in the gassy rims of these basalts, which range from 30-40% around 63°N, to just a few % around 60-50°N, where the water depth drops progressively from 1 km to 4 km (Fig. 2; Moore and Schilling, 1973; Schilling et al., 1983). The S contents of the subaerially erupted Iceland basalts are less than 100 ppm (6-97 ppm). As shown later in section 7, these basalts have lost >90% of their S by degassing, whereas the 5 sub-glacially erupted Iceland basalts range from 480-715 ppm S, and have lost only about 50% of S by degassing. The essentially constant S content along the Reykjanes Ridge, until H_2O and other volatile degassing takes place, suggests sulfide-saturation of these MORB prior to eruption, as generally observed elsewhere (e.g., Czamanske and Moore, 1977; Mathez, 1976). Under such low-oxygen fugacity, sulfide-saturated conditions (Katsura and Nagashim, 1974; Wallace and Carmichael, 1992), the sulfur solubility and content of basaltic magma is dominantly controlled by the Fe content, as extensively discussed for other MORB (e.g., Czamanske and Moore, 1977; Haughton et al., 1974; Kanehira et al., 1973; Mathez, 1976; Moore and Calk, 1991; Peach et al., 1990). This is further confirmed by the very slight S increase from 50°N~62°N (Fig. 4a), which is also accompanied by an increase in FeO (Schilling et al., 1983). As expected, apart from the degassed Iceland basalts, the Reykjanes Ridge basalt sulfur contents are enriched relative to PUM estimates, suggesting that S is incompatible during partial melting (e.g., Lorand, 1991).

5.2. Selenium and Tellurium.

In contrast to sulfur, Figures 4b-c show that both Te and Se contents increase noticeably from 50°N toward Iceland, until again there is a decrease due to degassing of major volatiles

around 63°N (or ~250-500 m water depth), as also observed for sulfur, halogens, and water (Moore and Schilling, 1973; Nichols et al., 2002; Unni and Schilling, 1978). The fact that the trace volatiles Se and Te degassed around the same critical depth of degassing as S and H_2O suggests that Se and Te are fluxed out by the latter two major volatiles, without Se and Te necessarily reaching their vapor saturation levels, a mechanism that has been similarly proposed for Cl and Br (Unni and Schilling, 1978).

It should be noted that the decrease in Se and Te due to degassing is more progressive than that of S, possibly caused by the pronounced low-pressure silicate fractional crystallization taking place around the 63.5°N region noted earlier (Fig. 3). The fractionation is apparently sulfide-free at this late stage, as evident by the accompanying along-ridge regular increasing Cu trend over the region (Fig. 3), and from thin section examination and modal phenocryst abundance analyses (Schilling et al., 1983). We will return to this question in Section 9.

6. Comparison of S, Se and Te contents in pillow basalt interiors versus glass rims.

Table 1 lists 15 basalt samples where both the glassy rim and the pillow interiors were analyzed for their S, Se, and Te contents. Two samples are from sub-glacial eruptions over Iceland, 11 are from the Reykjanes Ridge, and 2 are from the MAR south of the Gibbs fracture zone (Fig. 5). First, it should be noted that the systematic interior/glassy basalt differences in S content may in part be due to analytical differences, possibly accuracy related, considering that two distinct analytical methods were used (i.e., electron microprobe vs. XRF; see Section 3.2), but this is not the case for Se and Te. Yet, in all three S, Se, and Te cases, the along-ridge relative variations for glasses and pillow-interiors are similar, thus corroborating the general spatial trends. The sulfur contents in the pillow interiors are generally lower than in the glassy rims. The Se content of the pillow interiors and the glassy rim are essentially identical in 6 of the 15 cases, and in 9 other cases lower in the pillow interiors, similar to S. As for the Te contents, the pillow interiors are essentially identical to the glassy rims in 9 cases, but higher in 5 cases, and lower only in 1 case. A similar comparison has been made on 5 glass/pillow interior MORB pairs from the South Mid-Atlantic Ridge (Lissner et al., 2014). Their results are comparable and show no systematic differences with ours.

Lower contents of the halogens F and Cl in pillow interiors relative to glass rims were also observed on the same Reykjanes Ridge samples by Rowe and Schilling (1979) and Schilling et al. (1980). Corliss (1971) also noted this tendency in other submarine regions for elements such as Fe, Mn, Co, REE, Cu, and Pb. The loss of S and Se, but not Te, from the pillow interiors may be caused by the slow cooling and crystallization of the magma, making it possible for the S and Se to partition into residual fluids. These deuteric residual liquors may then be sequestered by oxidizing hydrothermal circulation of seawater (or glacial meltwater) through micro-cracks and fissures in these pillow basalts (Corliss, 1971; Rowe and Schilling, 1979; Schilling et al., 1980). Further support for this process comes from experimental evidence that indicates that sulfur will preferentially partition into a hydrous fluid rather than remain in the silicate melt (Keppler, 1999). Upon rock and/or sulfide oxidation, S is also known to be most mobile in ground waters or hydrothermal fluids, followed by Se, and least Te (e.g., Auclair et al., 1987; Dreibus et al., 1995; König et al., 2012; Lorand and Alard, 2010).

The higher content of tellurium in some of the pillow interiors may indicate that either the pillow interior has not lost any Te, or occasionally that Te was added to it from seawater circulation in micro-cracks upon cooling. In the seawater column, dissolved "conservative" S (content ~905 ppm) is present as S^{6+} in the form of sulfate (SO_4^{2-}), with a residence time of the order of 10^5 years. Dissolved Se with a "nutrient-type" distribution with depth is normally present as Se^{6+} selenate (SeO_4^{2-}) and Se^{4+} selenite (SeO_3^{2-}). Its total Se content ranges typically from ~0.5 to 0.18 ppb from surface to deep water (Measures and Burton, 1980; Measures et al., 1980), with a residence time of the order of 10^3 -10^5 years (Donat and Bruland, 1995). Similar to Se, Te also occurs as Te^{4+} and Te^{6+} species although in the 6+ state Te is instead present as a hydrosilate $Te(OH)_6$ rather than an oxyanion like SeO_4^{2-} (Lee and Edmond, 1985). Contrary to Se, Te is very reactive and rapidly scavenged by marine particulates, in particular Fe-Mn colloids and Fe-Mn deposits on the ocean floor (Hein et al., 2003; Koschinsky et al., 2004) and thus dissolved Te has a "scavenging-type" distribution with depth, with a residence time of $<10^3$ years. The total dissolved Te concentration in seawater, from surface to deep water, ranges from 0.153-0.19 ppt to 0.075-0.05 ppt (Donat and Bruland, 1995; Lee and Edmond, 1985). Possibly,

this observation might account for the small increase of Te in some of the pillow basalt interiors relative to glass in some of the samples analyzed.

7. Iceland mantle plume-DUM mixing considerations.

The progressive enrichments of Se and Te up to the point of degassing are roughly 4-5 for Te and 2-2.5 for Se, as also observed for other incompatible refractory elements such as the light REE (Schilling et al., 1983) and for higher incompatibilities such as Nb (Hanan et al., 2000; Kelley et al., 2013). A reasonable deduction would be that the Se and Te gradients of these undegassed basalts (i.e., 50°N to 62.5°N) are attributed to mantle mixing between the Iceland mantle plume, which is richer in Se and Te than the DUM, as previously indicated by Pb-Sr-Nd-Hf isotope and La/Sm ratio variations (Blichert-Toft et al., 2005; Hart et al., 1973; Schilling, 1973; Sun et al., 1975). We were not able to find any meaningful correlations between Se, Te, and Te/Se ratio with Pb-Sr-Nd-Hf isotope and La/Sm ratios (linear fits correlation coefficients R^2 range from 0.09 to 0.53). This is not all surprising considering that Se and Te are affected by partial melting and fractional crystallization effects, whereas Pb-Sr-Nd-Hf isotope ratios are usually not. Another reason for the absence of correlations is that the mixing gradients in the case of isotope ratios (e.g., $^{206}Pb/^{204}Pb$ in Fig. 2) extend southward from Iceland only to 60°N, as also illustrated by the symbol subdivision between Iceland, TMORB and NMORB, first based on La/Sm variation (Schilling, 1973). In contrast, the gradients in Se and Te appear broader, and extend at least to the Gibbs fracture zone, similar to the $^3He/^4He$ gradient (Fig. 2) and the thermal influence of the Iceland mantle plume (judging from the ridge axis elevation shown in Figure 2 and the numerical dynamic and thermal plume dispersion models of White and McKenzie (1995) and Ito et al. (1999).

Selenium, tellurium, and Te/Se ratios from the 50°N-62.5°N undegassed basalt population correlate linearly with $^3He/^4He$ ratios, with correlation coefficients (R^2) of 0.79, 0.69, 0.47, respectively. Similarly, the linear correlation for ridge-axis elevation versus $^3He/^4He$ ratio gives R^2 of 0.80. Copper also correlates linearly with $^3He/^4He$ ratio (R^2=0.82). Furthermore, the co-variation of Cu with MgO (Fig. 6) shows that increasing Cu in Iceland basalts and T-MORB correlates weakly with decreasing MgO, whereas among N-MORB there is no apparent

correlation, but at any MgO, the Iceland basalts are systematically higher than N-MORB, and the T-MORB lie in between. All these observations are consistent with the suggestion that the Iceland mantle plume may be richer in Te, Se and Cu, with a higher Te/Se ratio, than the DUM source.

The important difference in gradient scale-length between He and Pb-Sr-Nd-Hf isotope ratios has also been observed north of Iceland along the Kolbeinsey Ridge (Schilling et al., 1999). In this case, following Ito et al. (1999), we suggested that the upwelling Iceland mantle plume first encounters a complex OH-(C-CH_4-CO-CO_2) fluidization/de-fluidization zone involving He, resulting in an increase in its viscosity and enhancing its lateral spreading below its dry solidus. This proposed zone may well also involve redox conditions for C-species, OH and Fe^{3+}/Fe^{2+} (Bryndzia and Wood, 1990; Dixon and Stolper, 1995; Wood et al., 1990; Wood et al., 1996). Over the plume conduit at depths above the dry solidus, fractional melting and mixing would take place along the dispersing and decompressing plume flow-line beneath the ridge (see Fig.10 in Schilling et al., 1999). Could sulfides also be involved in this kind of incipient redox melting boundary? It is tempting to ascribe such an effect to the Reykjanes Ridge large-scale Se, Te, and Cu gradients, which are similar in scale to that of the thermal-related ridge-axis elevation and $^3He/^4He$ length-scale (compare Figures 2 and 4 over the 50°N-62.5°N region, and for Cu from 50-65°N). Considerable new information has appeared since on redox melting and the effect of the oxygen fugacity and carbon on deep incipient melting and volatile degassing beneath mid-ocean ridges and mantle plumes such as Iceland (e.g., Cottrell and Kelley, 2013; Dasgupta and Hirschmann, 2006; 2010; Dasgupta et al., 2007; Frost and McCammon, 2008; Keppler et al., 2003; Rohrbach et al., 2007; Rohrbach and Schmidt, 2011; Stagno et al., 2013). No clear conclusion can yet be drawn from these studies regarding the fate of sulfides. A geochemical rationale for coupling the Se and Te (and PGE and Cu) sulfide bearing component with this C-He spreading transport model of the Iceland mantle plume remains elusive and speculative at this point.

8. Relative extents of S, Se, Te basalt degassing.

On a relative basis, Figures 4 and 7 together indicate that the extent of degassing of the Iceland basalts decreases in the following order: greatest for S, followed by Te and least for Se.

At least three other methods can provide semi-quantitative estimates of the percent of volcanic degassing of these volatiles:

1) The most direct method is by comparing the average S, Se, or Te content of the un-degassed glasses closest to Iceland to those degassed on Iceland (e.g., Unni and Schilling, 1978). On this basis, the Iceland basalts have lost on average 95% of S, 86% of Te and 66% of Se.

2) Northward linear extrapolation over Iceland of the S, Se, and Te trend of un-degassed basalts along the Reykjanes Ridge south of 62.5°N (i.e., >600m water depth) relative to the actually observed degassed Iceland basalts yields on average 96% for S, 76% for Te and 69% for Se. The extents of degassing of S, Se, and Te by these first two methods are in reasonably good agreement, considering the uncertainties.

3) Another often used possibility is to compare a MORB volatile to a proxy refractory lithophile trace element with similar incompatibility, e.g., K or Ce for H_2O (Danyushevsky et al., 2000; Dixon et al., 2002; Michael, 1988; 1995; Simons et al., 2002), Nb for CO_2 (Cartigny et al., 2008; Saal et al., 2002), or Ba for Cl and Br (Schilling et al., 1980). Least-square linear correlations approaching zero between a proxy refractory lithophile trace element (x) versus Se, or Te, relative to this refractory proxy x, would determine the best non-volatile proxy. Of course, only the un-degassed basalts south of ~63°N are considered in the case of the Reykjanes Ridge. We were not able to find such proxies because of the shorter gradient in the refractory elements in comparison to that of Se and Te noted earlier. The closest proxy found was Cu, because its latitudinal trend along the Reykjanes Ridge is similar to Se and Te, up to where degassing takes place for Se and Te, but not Cu, which keeps increasing toward and over Iceland (compare Figures 3 and 4).

9. Fractional crystallization effects.

The along-ridge Se and Te contents of the un-degassed Reykjanes Ridge basalts do not parallel that of the Mg-values nor Ni (Figs. 3 and 4). The Se and Te of both N-MORB and T-MORB scatter broadly and overlap without any apparent trends over the entire range from Mg-values from 46 to 69. This is not surprising, since all the samples are spatially distant from each other and not likely to be genetically consanguineous. We propose that the progressive increase

in Se and Te shown in Figure 4 is not caused by the large, low-P-T, olivine-plag-cpx crystallization effects observed around 63.5°N (Hermes and Schilling, 1976), and is essentially free of sulfide fractionation for the following reasons. The undegassed Se and Te trends along the Reykjanes Ridge are similar to that of Cu, which has a comparable chalcophile behavior (Fig. 3). At the onset of H_2O, S, and other vapor/met related volatile degassing, however, Se and Te appear to partition into the vapor, whereas Cu keeps increasing toward Iceland without being affected either by degassing or by low pressure, late stage silicate crystallization effects. On either side of the 63.5°N minima in Ni and Mg# (Fig. 3), which correspond to the maximum in low T-P silicate crystallization, Cu in both T-MORB and Iceland basalts correlates negatively with MgO. This suggests that the effective bulk crystal/melt partition coefficient for Cu is less than unity (i.e., it exhibits incompatible behavior) for an oliv-cpx-plag crystallizing assemblage in a 1:2:3 ratio (Hermes and Schilling 1976). In contrast, Cu in N-MORB is uncorrelated with MgO (Fig.6). Sulfide liquid/silicate melt partition coefficients for Cu are 1623-1317 for basaltic melts in the range 7-9 wt. % MgO, respectively (Brenan, in revision). Some sulfide removal is apparent in N-MORB south of 54°N, as also observed from Ir and Pd variations on the same samples, which are much more influenced by sulfides than Se, Te and Cu (Schilling and Kingsley, in preparation). PGE sulfide liquid/silicate melt partition coefficients are 2-3 orders of magnitude greater than those of Cu, Se and Te (Bézos et al., 2005; Momme et al., 2003; Mungall and Brenan, 2014; Rehkämper et al., 1999). Bézos et al. (2005) estimated an immiscible sulfide melt segregation fraction, $X_{sulfide}$, of 120 ppm from the Pd content of a pair of N-MORB from the Kolbeinsey Ridge north of Iceland, ranging from 10 to 7 wt% MgO. This corresponds to 54% crystallization of oliv-plag-cpx and results in a sulfide segregation rate of 2 ppm/%FC (i.e., FC is fractional crystallization). Their model assumes that no PGE partitioned into the silicate assemblage (i.e., any silicate or oxide crystal/melt PGE partition coefficients are zero), and uses a $K^{sulfide/silicate\ melt}$ of 35,000 for Pd.

For comparison, using the same model, it can be shown that bracketing the positive PGE vs. MgO trends for the N-MORB from 50-54°N (Schilling and Kingsley, in prep) would require a maximum sulfide melt segregation fraction of only 5-9 ppm or 17-36 ppm, based on their Ir and Pd contents, respectively (corresponding to a sulfide segregation of 0.1-0.3 ppm/%FC and

0.3-1.2ppm/%FC). Our assessment uses two pairs of Reykjanes ridge N-MORB in a similar range of MgO (7-9 wt.%). The two basalt pairs are: 1) the "initial" melt, TR 100 23D-10g, which reaches the closely located "residual" basalt melt EN025 1D-1g by ~37% oliv.-plag.-cpx crystallization, and 2) the "initial" melt TR138 7D-1Ag, located south of the Gibbs FZ, which reaches the same "residual" melt EN025 1D-1g by ~53% silicate crystallization. The significant discrepancy between the sulfide removal rate estimate of Bézos et al. (2005) and ours is due to the fact that we used the PGE partition coefficients, $K^{sulf.\ liq./sil.melt}$, most recently reported by Mungall and Brenan (2014) which are 1-2 orders of magnitude higher. Based on this analysis, we conclude that the observed Se and Te data need not be corrected in any significant way for immiscible sulfide segregation. In the remaining discussion, we will assume that only the local scatter about the two large-scale, along-ridge Se and Te trends observed in Figures 4b-c may be caused by fractional crystallization effects, sulfide-bearing or not, and that the large-scale trends are not predominantly driven by such effects.

10. Partial melting effects.

Crustal thickness, ridge depth and CaO/Al_2O_3 ratio variations with latitude can be used as a proxy for the variation of the degree of partial melting (F) along the Reykjanes Ridge. The CaO/Al_2O_3 ratio in MORB inversely correlates with ridge depth and inversely with F. This relationship holds until clinopyroxene in the mantle source is exhausted over hotspots (Brodholt and Batiza, 1989; Klein and Langmuir, 1987; Klein and Langmuir, 1989; Niu and Batiza, 1991). This is indeed also the case along the Reykjanes Ridge, where the CaO/Al_2O_3 ratio increases with latitude and decreasing ridge depth, until Iceland is reached and the relationship breaks down (Schilling et al., 1983; Sigurdsson, 1981). In view of this complication, we instead use as a proxy for partial melting the thermal melting model of White and McKenzie (1995). Their model assumes a 200°C excess temperature for the Iceland plume and a melt thickness (basaltic crust) increasing from ~7km for normal oceanic crust thermally unaffected by the hotspot to ~21km over the center of Iceland (see their Fig. 4). Empirically, we have scaled this crustal variation to a linear increase in F with latitude (°N), namely $F = 0.066 + 0.00827(Lat.°N-50)$. In other words, normal crust near 50°N is produced by a mean F of about 7%, and over Iceland by 19%. On this

basis, as a function of such modeled degree of melting, Figure 7 shows the variation of S/Se, S/Te and Se/Te, normalized to primitive upper mantle (PUM) values (i.e., BSE estimates of S= 250 ppm, Se=75 ppb, and Te=12 ppb; McDonough and Sun, 1995). All the Reykjanes Ridge basalts have $(S/Se)_N$ ratios slightly greater than the PUM and $(S/Te)_N$ ratios significantly greater. The $(Se/Te)_N$ ratios are also greater than the PUM, primarily because of their lower Te content relative to PUM in undegassed MORB.

Considering only the undegassed basalt glasses, and assuming only a uniform PUM source with a sulfur content as in BSE, the combined progressive increase of Se and Te (Fig. 4b-c), and decrease in S/Se, S/Te and Se/Te ratios with increasing melting toward Iceland (Fig. 7) would suggest that Se is more compatible than S during mantle melting, and Te even more so. Sulfur has been estimated to have an effective bulk mantle/melt partition coefficient (D; residual solid/melt) on the order of 0.2-0.3 (as Al_2O_3) and is usually considered incompatible (e.g., Lorand, 1991). The decrease in Reykjanes Ridge S/Se, S/Te and Se/Te ratios with inferred increasing degree of melting is complementary and consistent with constraints on partial melting of Pyrenean peridotites (König et al., 2012; Lorand and Alard, 2010). These rocks are considered as residual mantle sources of basalts, ranging in composition from lherzolite to harzburgite with increasing degree of melting. Effective bulk D's during their melting have been estimated to be on the order of 0.2-0.3 for S and 1.4 for Se and Te. The Se/Te ratio variation in Figure 7 further indicates that the effective bulk partition coefficient D for Te must be greater than that for Se. A more quantitative approach to this single sulfide bearing PUM melting model is evaluated next, along with more quantitative constraints on the partitioning of Se and Te during partial melting beneath the MAR region.

11. Sulfide-bearing PUM melting models.

Congruent and incongruent melting models of a "sulfide bearing" single mantle source of PUM composition (i.e., BSE, 250 ppm sulfur, 714 ppm sulfide) are considered here, assuming that Se and Te are uniquely hosted in sulfides in the PUM, and the silicate or oxide crystal/melt partition coefficients are all zero, as has been previously assumed for PGE (e.g., Bockrath et al., 2004; Rehkämper et al., 1999).

11.1 Congruent sulfide melting.

Figures 7a-b show the variations of PUM normalized $(Se)_N$ and $(Te)_N$ observed in basalts from the Reykjanes Ridge and Iceland as a function of F. Superimposed on Figure 8 are partial melting models similar to Rehkämper et al. (1999). These models assume incremental partial melting of sulfide-bearing mantle of PUM composition, with continuous 0.1% residual melt retention. Both a columnar and a pooled triangular decompression-flow melting model are considered. The models assume that the Se and Te silicate (and oxide) partition coefficients, $K^{crystal/melt}$, are all zero, and consider distinct Se and Te $K^{sulfide\ liquid/silicate\ melt}$ partition coefficients. Exhaustion of sulfide occurs at F=20% in this sulfide-bearing PUM model. Figure 8 shows that a combination of the two dynamic flow melting models could satisfactorily span the $(Se)_N$ and $(Te)_N$ range of undegassed basalt variation with F, provided that the $K^{sulfide\ liquid/silicate\ melt}$ for Se is in the range of 10^3-10^4, and for Te is in the range of 10^4 –10^5. Consistently, the undegassed basalt $(Se/Te)_N$ variation is also well modeled if $K^{sulfide\ liquid\ /silicate\ melt}$ for Se is 10^3 and for Te is 10^4 (Fig 8c). The required $K^{sulfide\ liquid\ /silicate\ melt}$ partition coefficients are in remarkably good agreement with those recently published by Brenan (in revision), who reports $K^{sulfide\ liquid\ /silicate\ melt}$ in the range of 1623-1317 for Se and 14,914-12,332 for Te, for basaltic melts in the range of 7-9 wt% MgO. The corresponding initial weighted bulk partition coefficients, D_0, would be 1.16-0.95 for Se and 10.6-8.8 for Te under this assumed PUM sulfide-melting model. Thus Se would behave mostly as a very slightly incompatible/compatible element, whereas Te would be clearly compatible during this sulfide-bearing melting process. Patten et al. (2013) report coexisting sulfide globule/silicate glass partition coefficients for Se, $K^{globule\ sulfide\ /silicate\ melt}$, measured in MORB that are lower than these by as much as a factor of 3. These lower values are not considered further here (see the Supplement Section).

Based on the congruent sulfide-bearing melting model just discussed (with its inherent assumptions and qualifications) there appears no real need to invoke significantly distinct Se, Te, or S contents of the Iceland mantle plume relative to the surrounding DUM. Yet, mixing of the two sources, based on Pb-Nd-Sr-Hf and He isotope variations and the correlations of these with

Se, Te and Cu discussed in Section 7, remains valid as well. Salters and Stracke (2004) suggested that the DUM may be significantly depleted in sulfur (119 ppm) relative to the single-source BSE used in our modeling (i.e., 250 ppm for the PUM). Using their 119 ppm S in our Reykjanes Ridge melting model would require sulfide exhaustion at F=9.5%, which would occur at 53.5°N. As F increases northward along the ridge, erupting N-MORB would be sulfide undersaturated. With increasing melting, Se and Te would decrease progressively northward, which is opposite of the observed trends (Fig. 4), and sulfur would not remain constant as observed in Figure 4. This proposed very low sulfur content for the DUM thus does not appear likely, at least for the region considered here.

11.2 Incongruent sulfide melting.

PGE-constrained models of basalt generation by incongruent melting of a sulfide-bearing PUM, involving a monosulfide solid solution (Mss) coexisting with an immiscible sulfide melt, have been considered in broad terms by Mitchell and Keays (1981), Fryer and Greenough (1992), Greenough and Owen (1992), Ballhaus (1995), and Alard et al. (2000). Here, we consider the quantitative incongruent sulfide-bearing PUM melting model of Bockrath et al. (2004) and Ballhaus et al. (2006) for the case of Se and Te. Their model involves formation of a residual Mss phase coexisting with an immiscible sulfide melt, which is physically entrained and diluted with increasing degree of silicate melting. According to this physical, non-equilibrium model, they point out that PGE behave as incompatible elements with increasing silicate melting. Testing of this model requires knowing $K^{Mss/sulfide\ melt}$ for Se and Te. To our knowledge, only two such experimental Se and Te partitioning studies have been reported (Brenan, in revision; Helmy et al., 2010). For comparable metal/S ratios in Mss ranging from ~ 0.9-1, an average (n=5) of $K^{Mss/sulfide\ melt}$ of 0.67 for Se and 0.028 for Te are obtained and adopted. Note that the ratio of $K^{Mss/sulfide\ melt}$ partition coefficients for Se/Te is >1, whereas the ratio $K^{sulfide\ liquid\ /silicate\ melt}$ for Se/Te is <1, thus predicting opposite Se/Te fractionations. Figure 9 shows the variation of $(Se)_N$ and $(Te)_N$ as a function of mantle silicate melt fraction (F) using the two adopted $K^{Mss/sulfide\ melt}$ partition coefficient averages and the Bockrath et al. (2004) sulfide-incongruent and silicate

batch melting model, over a melt fraction of sulfide ranging from 0.1 to 1 (Bockrath et al., 2004 used 0.5). Regardless of the extent of incongruent sulfide melt fraction assumed, the trends are contrary to that observed along the Reykjanes Ridge, assuming increasing melting towards Iceland. According to this non-equilibrium physical model, the Se and Te concentrations would have to decrease toward the Iceland hotspot, which is opposite to what is observed (Figs. 4 & 9). This model is thus rejected for this region at least, as also evident from PGE variations in the same sample suite (Schilling and Kingsley, in prep).

12. Considerations of S, Se and Te recycling by plate tectonics.

An outstanding question remaining currently unanswered is how the Iceland mantle plume has become enriched in Se and Te relative to the DUM. We note that, with respect to broad deep-earth oceanic plate dynamic cycling and evolution, Se is enriched relative to BSE and increases northward from 1 to ~5, whereas Te is depleted and increases northward from 0.1 to 1 (Fig. 8). In the PUM congruent melting model considered above, both Se and Te have $K^{\text{sulfide liq./silicate melt}}$ partition coefficients much greater than unity, but their initial effective bulk partition coefficients, D_0, are 1.16–0.95 for Se and 10.7-8.8 for Te, until the sulfide phase is exhausted at F=20%. Thus, effectively, Se would behave mostly as a very slightly incompatible to compatible element, whereas Te would be clearly compatible during this sulfide-bearing melting process. For similar S-solubility (i.e., 1250 ppm), the threshold from incompatible to compatible, (i.e., D_0=1), requires $K^{\text{sulfide/silicate melt}}$ values of ~1400, 1750 and 2000, for initial mantle sulfur contents of 250, 200 and 175 ppm, with sulfide exhausted at melt fractions of 20, 16 and 14%, respectively. Thus, recurring partial melting could account in part for the discrepancy relative to BSE.

Based on incompatible trace elements and Nd-Sr-Pb-Hf isotope contents of modern basalts, it is commonly assumed that mantle plumes, such as Iceland, may represent the plate tectonic recycling of old (1.5-2 Gyr), hydrothermally altered oceanic crust (Hofmann and White, 1982), and possibly old lithosphere as well (Chauvel and Hémond, 2000). In contrast, the DUM must have a distinct and more complex history, more open system and partly complementary to early continental crust formation (e.g., Hofmann, 1997). How do these S, Se and Te observations

fit into such a recycling evolution?

To our knowledge, data on recycling of Se and Te by plate tectonics is practically nonexistent. On the other hand, the cycling of sulfur during oceanic crust hydrothermal alteration is better known. Near the ridge axis at high temperature, seawater sulfate intake combined with Ca causes extensive anhydrite precipitation, as well as reduction of sulfate to sulfide associated with oxidation of iron leached from the basaltic crust from Fe^{2+} to Fe^{3+}. On the other hand, diffuse low-temperature ridge flank hydrothermal circulation dissolves the anhydrite formed earlier. Budget calculations based on anhydrite and pyrite distribution from the Ocean Drilling Program Holes 504B and 735B, and corresponding S content and $\delta^{34}S$, suggest essentially no net change in the S content of the altered oceanic crust relative to MORB (Alt, 1995; Alt et al., 1986). At subduction zones, $\delta^{34}S$ in subaerial and submarine volcanic rocks are intermediate between a seawater and a MORB component (i.e., δ34S = 21‰, and ~0 ‰, respectively; Alt et al., 1993). The S enrichment in the mantle wedge may have been derived by fluid fluxing, either from the subducting sediments or the altered oceanic crust (e.g., see Alt et al., 1993; de Hoog et al., 2001; and references therein).

Judging from the evidence briefly discussed earlier in Section 6 and on comparative redox conditions of Se, Te and S, one might expect during such recycling that Se is likely to follow S, but Te may not. The Se/Te ratio of seawater is on the order of 300 to 3000 from surface to deep waters (e.g., Donat and Bruland, 1995). Undegassed Reykjanes Ridge basalts range from ~10-60. For comparison, BSE Se/Te=6.25 and C-1 chondrite Se/Te=9 (McDonough and Sun, 1995). These observed Se/Te fractionations not only reflect recurring partial melting but also redox processes during alteration of the oceanic crust and its recycling, including fluid release and melting at subduction zones during the plate tectonic cycle. Recent developments in S, Se, Te and Fe isotope fractionations during such plate tectonic recycling processes may provide new constraints on this important question (e.g., Rouxel, 2003; Rouxel et al., 2004; Rouxel et al., 2002; and references therein).

13. Conclusions.

1) There is little doubt that the S variation along the Reykjanes Ridge and its extension over Iceland, observed in Figure 3, is due to sulfide-saturation in ascending melts, until low hydrostatic pressures prevail and complex vapor-melt related volatile degassing of S, Se and Te, along with H_2O, Cl, and Br, takes place. S degassing is very extensive and abrupt, followed by Te and to a lesser extent Se.

2) Two major models were explored in order to account for the increases in Se, Te, and Te/Se observed in undegassed MORB from 50°N-62.5°N: a model of increasing melting of a single sulfide-bearing primary upper mantle source (PUM) toward the Iceland hotspot, and/or a model of along-ridge dilution of the Iceland mantle plume with the depleted upper mantle (DUM), as previously inferred from Pb-Sr-Nd and He isotope variations of the same basalts. The two models are not mutually exclusive. The former is viable provided that 1) the degree of partial melting along the Reykjanes Ridge increases northward from 7-19% (White et al. (1995)), and 2) the Se and Te sulfide melt/silicate melt partition coefficients required are as high as reported by Brenan (in revision). The latter model is supported by the correlation of Se, Te and Te/Se of the undegassed MORB population with $^3He/^4He$ ratios, as well as the correlation of Cu with $^3He/^4He$ from 50°N-65°N. It remains uncertain to what extent each of these two models dominates the Se, Te, and Cu variations observed, considering the inherent uncertainties in the model parameters involved.

3) Relative to BSE, Se in the undegassed basalts is enriched and increases northward from 1 to ~5 (Fig. 7a), whereas Te is depleted and increases northward from 0.1 to 1 (Fig. 7b). Recurring partial melting during the open evolution of the DUM and the Iceland mantle plume could not alone account for this discrepancy, since, as previously pointed out, Se acts slightly incompatibly and Te compatibly during this process. Prior to this latest melting event, some opposite fractionation between Se and Te relative to BSE would have to have occurred at some point during the open evolution of the DUM and that of the Iceland mantle plume. Clearly, the distinct redox conditions of S, Se and Te during plate alteration by seawater and its recycling at

subduction zones also warrant further consideration.

4) Finally, we have noted in Section 7 distinct mixing gradient length scales. Longer mixing length scales are observed for Se, Te, $^3He/^4He$, Cu, and PGE, coincident with the thermally related ride-axis elevation gradients, whereas Nd-Sr-Hf-Pb isotopes, La/Sm and other refractory incompatible trace elements (e.g., Th and Nb), and other volatile elements south of 63°N (e.g., H_2O and halogens) apparently mix over a shorter length scale along the ridge, and this contrast remains poorly understood and needs further evaluation. We have briefly suggested a possible cause by deep incipient redox melting, devolatilization and C-He transport beneath the MAR-Iceland region. The possible involvement of sulfide with such an effect is tempting, but speculative. These mixing gradient length-scale distinctions need to be further documented and explored.

Acknowledgments

We thank R. Kingsley, J.M. Rhodes, and C. Mandeville for assistance with analyses. This work was supported by NSF award OCE# 0326658 to JGS. NSF award OCE# 1258771 provides curatorial support for marine geological samples at the Graduate School of Oceanography, University of Rhode Island.

List of Tables

Table 1. S, Se and Te contents of basalts from the Reykjanes Ridge and SW Iceland Rift Zone

Figure Captions

Figure 1. Regional map of Iceland and the Reykjanes ridge. Basalt sample locations for this study are shown as circular symbols along the Reykjanes ridge and extension over the Iceland SW Neovolcanic Zone. Color coding is based on the mixing model of the Iceland mantle plume

with the depleted upper mantle, based on variation in $(La/Sm)_N$ (Schilling, 1973; Schilling et al., 1983). Red circles are for Iceland subaerially erupted basalts and 5 subglacial basalt glasses. Blue circles are for depleted N-MORB samples. Green circles are for the mixing zone T-MORB samples. This map was generated in GeoMapApp (www.geomapapp.org) using version 2.6 of the Global Multi-Resolution Topography synthesis base map of Ryan et al. (2009).

Figure 2. Reykjanes Ridge and Iceland basalt latitudinal variations in (a) $^{206}Pb/^{204}Pb$, (Blichert-Toft et al., 2005), (b) $^{3}He/^{4}He$ (R/Ra; Kurz et al., 1985; Poreda et al., 1986), and (c) sample elevation. Color coding is based on the mixing model of the Iceland mantle plume with the depleted upper mantle based on $(La/Sm)_N$ variation (Schilling, 1973; Schilling et al., 1983). As on Figure 1, red circles are for subaerial/subglacial Iceland basalts, blue circles are for N-MORB, and green circles are for T-MORB from the mixing zone. Vertical, red dotted line denotes the position of sea level and separates subaerial/subglacial samples from those erupted in the submarine environment. Vertical, blue dashed line denotes the latitude of the Gibbs fracture zone.

Figure 3. Reykjanes Ridge and Iceland basalt latitudinal variations in (a) Cu, (b) Ni, and (c) Mg-value (Kelley et al., 2013; Schilling et al., 1983; Sigurdsson, 1981). Note the minimum in both Ni and Mg-value around 63.5°N, which is not apparent for Cu. Symbol and vertical line colors are the same as in Fig. 2.

Figure 4. Reykjanes Ridge and Iceland basalt latitudinal variations in (a) S, (b) Se, and (c) Te concentrations. Note on panel (a) that only submarine glass S concentrations are shown. Symbol and vertical line colors are the same as in Figure 2. The circles are for glasses and submarine whole-rock samples, including 5 subglacial Iceland basalt glasses (see Table 1), whereas diamonds are for subaerial Iceland basalts.

Figure 5. Comparison of S, Se and Te contents of glassy rims (closed circles) and pillow interiors (open diamonds) of 15 pillow basalts studied along the Reykjanes Ridge and Iceland SW Rift Zone. Symbol and vertical line colors are the same as defined in Figure 2

Figure 6. Reykjanes Ridge and Iceland basalt variations of Cu as a function of MgO. As on Figure 1, red circles are for subaerial/subglacial Iceland basalts, blue circles are for N-MORB, and green circles are for T-MORB from the mixing zone. Least-squares linear regressions through these 3 groups have correlation coefficients R^2 of 0.21 (long-dashed line; n=17), 0.21 (dotted line; n=31) and 0.004 (solid line; n=20), respectively.

Figure 7. Reykjanes Ridge and Iceland basalt variations of (a) S/Se_N, (b) S/Te_N, and (c) Se/Te_N, normalized to bulk silicate Earth (BSE), as a function of the degree of partial melting (melt fraction; F). F is assumed to increase linearly with latitude °N (i.e., F = 0.066 + 0.00827 (Lat.°N – 50), modified after the thermal melting model of White and McKenzie (1995). See text for justification. The BSE estimated values used are those of McDonough and Sun (1995). Symbol and vertical line colors are the same as in Figure 2. The circles are for glasses and submarine whole-rock samples, including 5 subglacial Iceland basalt glasses (see Table 1), whereas diamonds are for subaerial Iceland basalts.

Figure 8. Reykjanes Ridge and Iceland basalt variations of (a) Se_N, (b) Te_N, and (c) Se/Te_N, normalized to bulk silicate Earth (BSE; McDonough and Sun, 1995), as a function of melt fraction (F; as assumed and used in Figure 7). Symbol colors are the same as in Figure 2 and the circles are for glasses and submarine whole-rock samples, including 5 subglacial Iceland basalt glasses (see Table 1), whereas diamonds are for subaerial Iceland basalts. Superimposed are columnar (solid lines) and triangular (dotted lines) flow melting models of a sulfide bearing mantle of PUM composition, modified after Rehkämper et al. (1999) in the following way. We used a non-modal batch melting model with a continuous retention of 0.001 melt fraction. Results are hardly distinguishable from their model. For Se in panel (a), conditions used, up to F= 20% when the mantle sulfide is exhausted, are:

Phases (j):	Silicate Solid	Retained Melt	Sulfide	Sulfur (ppm)
K_j:	0	1	10^2 to 10^4	
Solid (xo_j):	0.994286	0.001	0.000714*	250
Melt (p_j):	0.99643		0.003571*	1250

* assuming 35% S in sulfide

where K_j is the Se partition coefficient of phase j/silicate melt, xo_j is initial solid fraction of phase j, and p_j is the constant melt fraction of phase j entering the melt during melting. Note that K (sulfide/silicate melt) on the order of 10^3 to 10^4 would satisfy the undegassed N-MORB and T-MORB Se variation observed along the Reykjanes Ridge, regardless of whether a triangular or columnar melting zone is considered. For Te in panel (b), conditions are the same except that K (sulfide/silicate melt) for Te on the order of 10^4 to 10^5 is needed to span the un-degassed N-MORB and T-MORB Te variation observed along the Reykjanes Ridge, regardless of whether a triangular or columnar melting zone is considered. In panel (c), the Se/Te_N ratios for undegassed basalts from the Reykjanes Ridge are spanned and confined by triangular and columnar melting models with bulk K(sulfide/silicate melt) of 10^3 for Se and 10^4 for Te.

Figure 9. Reykjanes Ridge and Iceland basalt variations of (a) Se_N and (b) Te_N, normalized to bulk silicate Earth (BSE; McDonough and Sun, 1995) as a function of melt fraction (F; as assumed and used in Figure 7). Symbol colors are the same as in Figure 2 and the circles are for glasses and submarine whole-rock samples, including 5 subglacial Iceland basalt glasses (see Table 1), whereas diamonds are for subaerial Iceland basalts. Superimposed is the non-equilibrium physical incongruent sulfide-bearing PUM melting model of Bockrath et al. (2004) and Ballhaus et al. (2006). The different curves refer to the weight fractions of sulfide (F_{sul}) initially being melted according to their model. They assumed 0.5. Note that the trends predicted by this model are opposite to that observed along the Reykjanes Ridge, assuming that melting increases toward the Iceland plume. For Te_N, in (b), the model curves do not even cover the data span observed.

References

Alard, O., Griffin, W.L., Lorand, J.P., Jackson, S.E., O'Reilly, S.Y., 2000. Non-chondritic distribution of the highly siderophile elements in mantle sulphides. Nature, 407(6806): 891-894, doi: 10.1038/35038049.

Alt, J.C., 1995. Sulfur isotopic profile through the oceanic crust: Sulfur mobility and seawater-crustal sulfur exchange during hydrothermal alteration. Geology, 23(7): 585-588.

Alt, J.C., Honnorez, J., Laverne, C., Emmermann, R., 1986. Hydrothermal alteration of a 1 km section through the upper oceanic crust, Deep Sea Drilling Project Hole 504B: Mineralogy, chemistry, and evolution of seawater-basalt interactions. Journal of Geophysical Research, 91(B10): 10309-10355.

Alt, J.C., Shanks, W.C., III, Jackson, M.C., 1993. Cycling of sulfur in subduction zones: The geochemistry of sulfur in the Mariana Island Arc and back-arc trough. Earth and Planetary Science Letters, 119: 477-494.

Auclair, G., Fouquet, Y., Bohn, M., 1987. Distribution of Selenium in High-Temperature Hydrothermal Sulfide Deposits at 13-Degrees-North, East Pacific Rise. Canadian Mineralogist, 25: 577-587.

Ballhaus, C., 1995. Is the upper mantle metal-saturated? Earth and Planetary Science Letters, 132(1-4): 75-86, doi: 10.1016/0012-821X(95)00047-G.

Ballhaus, C., Bockrath, C., Wohlgemuth-Ueberwasser, C., Laurenz, V., Berndt, J., 2006. Fractionation of the noble metals by physical processes. Contributions to Mineralogy and Petrology, 152(6): 667-684, doi: 10.1007/S00410-006-0126-Z.

Barnes, S.J., Savard, D., Bedard, L.P., Maier, W.D., 2009. Selenium and sulfur concentrations in the Bushveld Complex of South Africa and implications for formation of the platinum-group element deposits. Mineralium Deposita, 44(6): 647-663, doi: 10.1007/S00126-009-0237-3.

Bézos, A., Lorand, J.P., Humler, E., Gros, M., 2005. Platinum-group element systematics in Mid-Oceanic Ridge basaltic glasses from the Pacific, Atlantic, and Indian Oceans. Geochimica Et Cosmochimica Acta, 69(10): 2613-2627, doi: 10.1016/J.Gca.2004.10.023.

Blichert-Toft, J. et al., 2005. Geochemical segmentation of the Mid-Atlantic Ridge north of Iceland and ridge-hot spot interaction in the North Atlantic. Geochem. Geophys. Geosyst., 6(1): Q01E19, doi: 10.1029/2004gc000788.

Bockrath, C., Ballhaus, C., Holzheid, A., 2004. Fractionation of the platinum-group elements during mantle melting. Science, 305(5692): 1951-1953, doi: 10.1126/Science.1100160.

Brenan, J.M., in revision. Se-Te fractionation by sulfide–silicate melt partitioning: Implications for the composition of mantle-derived magmas and their melting residues. Earth and Planetary Science Letters.

Brodholt, J.P., Batiza, R., 1989. Global Systematics of Unaveraged Mid-Ocean Ridge Basalt Compositions - Comment. Journal of Geophysical Research-Solid Earth and Planets, 94(B4): 4231-4239, doi: 10.1029/Jb094ib04p04231.

Bryndzia, L.T., Wood, B.J., 1990. Oxygen thermobarometry of abyssal spinel peridotites: The redox state and C-O-H volatile composition of the Earth's sub-oceanic upper mantle. American Journal of Science, 290: 1093-1116.

Cartigny, P., Pineau, F., Aubaud, C., Javoy, M., 2008. Towards a consistent mantle carbon flux estimate: Insights from volatile systematics (H_2O/Ce, δD, CO_2/Nb) in the North Atlantic mantle (14° N and 34° N). Earth and Planetary Science Letters, 265(3-4): 672-685, doi: 10.1016/j.epsl.2007.11.011.

Chauvel, C., Hémond, C., 2000. Melting of a complete section of recycled oceanic crust: Trace element and Pb isotopic evidence from Iceland. Geochemistry Geophysics Geosystems, 1.

Corliss, J.B., 1971. Origin of Metal-Bearing Submarine Hydrothermal Solutions. Journal of Geophysical Research, 76(33): 8128-8138, doi: 10.1029/Jc076i033p08128.

Cottrell, E., Kelley, K.A., 2013. Redox Heterogeneity in Mid-Ocean Ridge Basalts as a Function of Mantle Source. Science, 340(6138): 1314-1317, doi: 10.1126/science.1233299.

Czamanske, G.K., Moore, J.G., 1977. Composition and Phase Chemistry of Sulfide Globules in Basalt from Mid-Atlantic Ridge Rift Valley near 37°N Lat. Geological Society of America Bulletin, 88(4): 587-599, doi: 10.1130/0016-7606(1977) 88<587:Capcos>2.0.Co;2.

Danyushevsky, L.V., Eggins, S.M., Falloon, T.J., Christie, D.M., 2000. H_2O abundance in depleted to moderately enriched mid-ocean ridge magmas; Part I: Incompatible behaviour, implications for mantle storage, and origin of regional variations. Journal of Petrology, 41(8): 1329-1364.

Dasgupta, R., Hirschmann, M.M., 2006. Melting in the Earth's deep upper mantle caused by carbon dioxide. Nature, 440: 659-662, doi: 10.1038/nature04612.

Dasgupta, R., Hirschmann, M.M., 2010. The deep carbon cycle and melting in Earth's interior. Earth and Planetary Science Letters, 298(1-2): 1-13, doi: 10.1016/j.epsl.2010.06.039.

Dasgupta, R., Hirschmann, M.M., Smith, N.D., 2007. Water follows carbon: CO_2 incites deep silicate melting and dehydration beneath mid-ocean ridges. Geology, 35(2): 135-138, doi: 10.1130/G22856a.1.

de Hoog, J.C.M., Mason, P.R.D., Van Bergen, M.J., 2001. Sulfur and chalcophile elements in subduction zones: Constraints from a laser-ablation ICP-MS study of melt inclusions from Galunggung Volcano, Indonesia. Geochimica et Cosmochimica Acta, 65(18): 3147-3164.

Dixon, J.E., Leist, L., Langmuir, C.H., Schilling, J.-G., 2002. Recycled dehydrated lithosphere observed in plume-influenced mid-ocean-ridge basalt. Nature, 420: 385-389.

Dixon, J.E., Stolper, E., 1995. An experimental study of water and carbon dioxide solubilities in mid-ocean ridge basaltic liquids. Part II. Applications to degassing. Journal of Petrology, 36(6): 1633-1646.

Donat, J.R., Bruland, K.W., 1995. Trace elements in the oceans. In: Steinnes, E., Salbu, B. (Eds.), Trace elements in natural waters. CRC Press, Boca Raton, FL, pp. 247-281.

Dreibus, G., Palme, H., Spettel, B., Zipfel, J., Wanke, H., 1995. Sulfur and Selenium in Chondritic Meteorites. Meteoritics, 30(4): 439-445.

DuFresne, A., 1960. Selenium and tellurium in meteorites. Geochimica et Cosmochimica Acta, 20(2): 141-148, doi: 10.1016/0016-7037(60)90056-9.

Eckstrand, O. et al., 1989. Preliminary data on sulphur isotopes and Se/S ratios, and the source of sulphur in magmatic sulphides from the Fox River Sill, Molson Dykes and Thompson

nickel deposits, northern Manitoba. Current Research Part C, Geological Survey of Canada, Paper: 235-242.

Fisk, M.R., 1978. Melting relations and mineral chemistry of Iceland and Reykjanes Ridge basalts. Doctoral Dissertation Thesis, University of Rhode Island, Kingston, RI, 254 pp.

Fisk, M.R., Schilling, J.G., Sigurdsson, H., 1980. An Experimental Investigation of Iceland and Reykjanes Ridge Tholeiites: 1. Phase-Relations. Contributions to Mineralogy and Petrology, 74(4): 361-374.

Forrest, A., 2005. Sulfur, Selenium and Tellurium in Reykjanes Ridge and Iceland Basalts, Uniersity of Rhode Island, Kingston, RI, 175 pp.

Forrest, A., Kingsley, R., Schilling, J.-G., 2009. Determination of Selenium and Tellurium in Basalt Rock Reference Materials by Isotope Dilution Hydride Generation-Inductively Coupled Plasma-Mass Spectrometry (ID-HG-ICP-MS). Geostandards and Geoanalytical Research, 33(2): 261-269, doi: 10.1111/j.1751-908X.2009.00841.x.

Frost, D.J., McCammon, C.A., 2008. The redox state of Earth's mantle. Annual Review of Earth and Planetary Sciences, 36: 389-420, doi: 10.1146/Annurev.Earth.36.031207.124322.

Fryer, B.J., Greenough, J.D., 1992. Evidence for Mantle Heterogeneity from Platinum-Group-Element Abundances in Indian-Ocean Basalts. Canadian Journal of Earth Sciences, 29(11): 2329-2340, doi: 10.1139/E92-181.

Greenland, L., Campbell, E., 1977. Variation of Se, Te, In, Tl and Zn with differentiation of tholeiitic magma. Neues Jahrbuch fur Mineralogie. Monatshathe: 12-119.

Greenough, J.D., Owen, J.V., 1992. Platinum-Group Element Geochemistry of Continental Tholeiites - Analysis of the Long-Range Dyke Swarm, Newfoundland, Canada. Chemical Geology, 98(3-4): 203-219, doi: 10.1016/0009-2541(92)90185-8.

Guo, J.F., Griffin, W.L., O'Reilly, S.Y., 1999. Geochemistry and origin of sulphide minerals in mantle xenoliths: Qilin, southeastern China. Journal of Petrology, 40(7): 1125-1149.

Hanan, B.B., Blichert-Toft, J., Kingsley, R., Schilling, J.G., 2000. Depleted Iceland mantle plume geochemical signature: Artifact of multicomponent mixing? Geochem. Geophys. Geosyst., 1(4): 1-19, doi: 10.1029/1999gc000009.

Hart, S.R., Schilling, J.-G., Powell, J.L., 1973. Basalts from Iceland and Along the Reykjanes Ridge: Sr Isotope Geochemistry. Nature, 246: 104-107, doi: 10.1038/physci246104a0.

Hattori, K.H., Arai, S., Clarke, D.B., 2002. Selenium, tellurium, arsenic and antimony contents of primary mantle sulfides. Canadian Mineralogist, 40: 637-650, doi: 10.2113/Gscanmin. 40.2.637.

Haughton, D.R., Roeder, P.L., Skinner, B.J., 1974. Solubility of Sulfur in Mafic Magmas. Economic Geology, 69(4): 451-467.

Hein, J.R., Koschinsky, A., Halliday, A.N., 2003. Global occurrence of tellurium-rich ferromanganese crusts and a model for the enrichment of tellurium. Geochimica Et Cosmochimica Acta, 67(6): 1117-1127, doi: 10.1016/S0016-7037(00)01279-6.

Helmy, H.M., Ballhaus, C., Wohlgemuth-Ueberwasser, C., Fonseca, R.O.C., Laurenz, V., 2010. Partitioning of Se, As, Sb, Te and Bi between monosulfide solid solution and sulfide melt - Application to magmatic sulfide deposits. Geochimica Et Cosmochimica Acta, 74(21): 6174-6179, doi: 10.1016/J.Gca.2010.08.009.

Hermes, O.D., Schilling, J.G., 1976. Olivine from Reykjanes ridge and Iceland tholeiites, and its significance to the two-mantle source model. Earth and Planetary Science Letters, 28(3): 345-355, doi: 10.1016/0012-821x(76)90196-5.

Hertogen, J., Janssens, M.J., Palme, H., 1980. Trace elements in ocean ridge basalt glasses: implications for fractionations during mantle evolution and petrogenesis. Geochimica et Cosmochimica Acta, 44(12): 2125-2143, doi: 10.1016/0016-7037(80)90209-4.

Hofmann, A.W., 1997. Mantle geochemistry: the message from oceanic volcanism. Nature, 385: 219-229.

Hofmann, A.W., White, W.M., 1982. Mantle plumes from ancient oceanic crust. Earth and Planetary Science Letters, 57: 421-436.

Ito, G., Shen, Y., Hirth, G., Wolfe, C.J., 1999. Mantle flow, melting, and dehydration of the Iceland mantle plume. Earth and Planetary Science Letters, 165(1): 81-96, doi: 10.1016/S0012-821x(98)00216-7.

Jenner, F.E., O'Neill, H.S.C., 2012. Analysis of 60 elements in 616 ocean floor basaltic glasses. Geochemistry Geophysics Geosystems, 13, doi: 10.1029/2011gc004009.

Kanehira, K., Yui, S., Sakai, H., Sasaki, A., 1973. Sulphide globules and sulphur isotope ratios in the abyssal tholeiite from the Mid-Atlantic Ridge near 30°N latitude. Geochemical Journal, 7(2): 89-96, doi: 10.2343/geochemj.7.89.

Katsura, T., Nagashim, S., 1974. Solubility of Sulfur in Some Magmas at 1-Atmosphere. Geochimica Et Cosmochimica Acta, 38(4): 517-531, doi: 10.1016/0016-7037(74)90038-6.

Kelley, K.A., Kingsley, R.H., Schilling, J.-G., 2013. Composition of plume-influenced mid-ocean ridge lavas and glasses from the Mid-Atlantic Ridge, East Pacific Rise, Galápagos Spreading Center, and Gulf of Aden. Geochemistry Geophysics Geosystems, 14(1), doi: 10.1002/ggge.20049.

Keppler, H., 1999. Experimental evidence for the source of excess sulfur in explosive volcanic eruptions. Science, 284(5420): 1652-1654, doi: 10.1126/Science.284.5420.1652.

Keppler, H., Wiedenbeck, M., Shcheka, S.S., 2003. Carbon solubility in olivine and the mode of carbon storage in the Earth's mantle. Nature, 424(6947): 414-416, doi: 10.1038/Nature01828.

Klein, E.M., Langmuir, C.H., 1987. Global correlations of ocean ridge basalt chemistry with axial depth and crustal thickness. Journal of Geophysical Research, 92(B8): 8089-8115.

Klein, E.M., Langmuir, C.H., 1989. Local versus global variations in ocean ridge basalt composition: A reply. Journal of Geophysical Research, 94(B4): 4241-4252.

König, S., Lissner, M., Lorand, J.-P., Bragagni, A., Luguet, A., 2015. Mineralogical control of selenium, tellurium and highly siderophile elements in the Earth’s mantle: Evidence from mineral separates of ultra-depleted mantle residues. Chemical Geology, 396(0): 16-24, doi: 10.1016/j.chemgeo.2014.12.015.

König, S., Luguet, A., Lorand, J.P., Wombacher, F., Lissner, M., 2012. Selenium and tellurium systematics of the Earth's mantle from high precision analyses of ultra-depleted orogenic peridotites. Geochimica Et Cosmochimica Acta, 86: 354-366, doi: 10.1016/J.Gca.2012.03.014.

Koschinsky, A., Hein, J.R., Bau, M., 2004. The importance of surface oxidation for the enrichment of Te and Se on Mn oxides and Fe oxyhydroxide. In: Wanty, R.B., Seal, R.R. (Eds.), Water-Rock Interaction. Balkema Publ., Leiden, pp. 1323-1326.

Kullerud, G., 1970. Sulfide phase relations, Mineralogical Society of America Special Paper. Mineralogical Society of America, pp. 199-210.

Kurz, M.D., Meyer, P.S., Sigurdsson, H., 1985. Helium Isotopic Systematics within the Neovolcanic Zones of Iceland. Earth and Planetary Science Letters, 74(4): 291-305, doi: 10.1016/S0012-821x(85)80001-7.

Laul, J.C., Anders, E., Morgan, J.W., Keays, R.R., Ganapath.R, 1972. Chemical Fractionations in Meteorites .5. Volatile and Siderophile Elements in Achondrites and Ocean Ridge Basalts. Geochimica Et Cosmochimica Acta, 36(3): 329-&, doi: 10.1016/0016-7037 (72)90027-0.

Lee, D.S., Edmond, J.M., 1985. Tellurium Species in Seawater. Nature, 313(6005): 782-785, doi: 10.1038/313782a0.

Lissner, M. et al., 2014. Selenium and tellurium systematics in MORBs from the southern Mid-Atlantic Ridge (47–50°S). Geochimica et Cosmochimica Acta, 144: 379-402, doi: 10.1016/j.gca.2014.08.023.

Lorand, J.P., 1991. Sulphide Petrology and Sulphur Geochemistry of Orogenic Lherzolites: A Comparative Study of the Pyrenean Bodies (France) and the Lanzo Massif (Italy). Journal of Petrology: 77-95.

Lorand, J.P., Alard, O., 2010. Determination of selenium and tellurium concentrations in Pyrenean peridotites (Ariege, France): New insight into S/Se/Te systematics of the upper in mantle samples. Chemical Geology, 278(1-2): 120-130, doi: 10.1016/J.Chemgeo. 2010.09.007.

Mathez, E.A., 1976. Sulfur solubility and magmatic sulfides in submarine basalt glass. Journal of Geophysical Research, 81(23): 4269-4276.

McDonough, W.F., Sun, S.S., 1995. The Composition of the Earth. Chemical Geology, 120(3-4): 223-253, doi: 10.1016/0009-2541(94)00140-4.

Measures, C.I., Burton, J.D., 1980. The Vertical-Distribution and Oxidation-States of Dissolved Selenium in the Northeast Atlantic-Ocean and Their Relationship to Biological Processes. Earth and Planetary Science Letters, 46(3): 385-396, doi: 10.1016/0012-821x (80)90052-7.

Measures, C.I., Mcduff, R.E., Edmond, J.M., 1980. Selenium Redox Chemistry at Geosecs-I Re-Occupation. Earth and Planetary Science Letters, 49(1): 102-108, doi: 10.1016/0012-821x(80)90152-1.

Michael, P., 1988. The concentration, behavior and storage of H_2O in the suboceanic upper mantle: Implications for mantle metasomatism. Geochimica et Cosmochimica Acta, 52: 555-566.

Michael, P., 1995. Regionally distinctive sources of depleted MORB: Evidence from trace elements and H_2O. Earth and Planetary Science Letters, 131(3-4): 301-320, doi: 10.1016/0012-821X(95)00023-6.

Mitchell, R.H., Keays, R.R., 1981. Abundance and Distribution of Gold, Palladium and Iridium in Some Spinel and Garnet Iherzolites - Implications for the Nature and Origin of

Precious Metal-Rich Intergranular Components in the Upper Mantle. Geochimica Et Cosmochimica Acta, 45(12): 2425-2442, doi: 10.1016/0016-7037(81)90096-X.

Momme, P., Oskarsson, N., Keays, R.R., 2003. Platinum-group elements in the Icelandic rift system: melting processes and mantle beneath Iceland (vol 196, pg 209, 2003). Chemical Geology, 201(1-2): 181-182, doi: 10.1016/S0009-2541(03)00191-8.

Moore, J., Schilling, J.-G., 1973. Vesicles, water, and sulfur in Reykjanes Ridge basalts. Contributions to Mineralogy and Petrology, 41(2): 105-118, doi: 10.1007/bf00375036.

Moore, J.G., Calk, L.C., 1991. Degassing and Differentiation in Subglacial Volcanos, Iceland. Journal of Volcanology and Geothermal Research, 46(1-2): 157-180, doi: 10.1016/0377-0273(91)90081-A.

Morgan, J.W., 1986. Ultramafic Xenoliths - Clues to Earths Late Accretionary History. Journal of Geophysical Research-Solid Earth and Planets, 91(B12): 2375-2387, doi: 10.1029/Jb091ib12p12375.

Mungall, J.E., Brenan, J.M., 2014. Partitioning of platinum-group elements and Au between sulfide liquid and basalt and the origins of mantle-crust fractionation of the chalcophile elements. Geochimica et Cosmochimica Acta, 125(0): 265-289, doi: 10.1016/j.gca.2013.10.002.

Nichols, A.R.L., Carroll, M.R., Hoskuldsson, A., 2002. Is the Iceland hot spot also wet? Evidence from the water contents of undegassed submarine and subglacial pillow basalts. Earth and Planetary Science Letters, 202(1): 77-87, doi: 10.1016/S0012-821x(02)00758-6.

Niu, Y.L., Batiza, R., 1991. An Empirical-Method for Calculating Melt Compositions Produced beneath Midocean Ridges - Application for Axis and Off-Axis (Seamounts) Melting. Journal of Geophysical Research-Solid Earth, 96(B13): 21753-21777, doi: 10.1029/91jb01933.

O'Neill, H.S.C., Palme, H., 1998. Composition of the silicate Earth: implications for accretion and core formation. The Earth's Mantle: Composition, Structure and Evolution, 1.

Patten, C., Barnes, S.J., Mathez, E.A., Jenner, F.E., 2013. Partition coefficients of chalcophile elements between sulfide and silicate melts and the early crystallization history of sulfide liquid: LA-ICP-MS analysis of MORB sulfide droplets. Chemical Geology, 358: 170-188, doi: 10.1016/J.Chemgeo.2013.08.040.

Peach, C.L., Mathez, E.A., Keays, R.R., 1990. Sulfide Melt-Silicate Melt Distribution Coefficients for Noble-Metals and Other Chalcophile Elements as Deduced from MORB - Implications for Partial Melting. Geochimica Et Cosmochimica Acta, 54(12): 3379-3389, doi: 10.1016/0016-7037(90)90292-S.

Poreda, R., Schilling, J.G., Craig, H., 1986. Helium and hydrogen isotopes in ocean-ridge basalts north and south of Iceland. Earth and Planetary Science Letters, 78(1): 1-17, doi: 10.1016/0012-821x(86)90168-8.

Rehkämper, M. et al., 1999. Ir, Ru, Pt, and Pd in basalts and komatiites: New constraints for the geochemical behavior of the platinum-group elements in the mantle. Geochimica Et Cosmochimica Acta, 63(22): 3915-3934, doi: 10.1016/S0016-7037(99)00219-7.

Rohrbach, A. et al., 2007. Metal saturation in the upper mantle. Nature, 449(7161): 456-458, doi: 10.1038/Nature06183.

Rohrbach, A., Schmidt, M.W., 2011. Redox freezing and melting in the Earth's deep mantle resulting from carbon–iron redox coupling. Nature, 472(7342): 209-212, doi: 10.1038/nature09899.

Rouxel, O., 2003. Iron isotope fractionation during oceanic crust alteration. Chemical Geology, 202(1-2): 155-182, doi: 10.1016/j.chemgeo.2003.08.011.

Rouxel, O., Fouquet, Y., Ludden, J.N., 2004. Subsurface processes at the Lucky Strike hydrothermal field, Mid-Atlantic Ridge: Evidence from sulfur, selenium, and iron isotopes. Geochimica Et Cosmochimica Acta, 68(10): 2295-2311, doi: 10.1016/J.Gca.2003.11.029.

Rouxel, O., Ludden, J., Carignan, J., Marin, L., Fouquet, Y., 2002. Natural variations of Se isotopic composition determined by hydride generation multiple collector inductively coupled plasma mass spectrometry. Geochimica Et Cosmochimica Acta, 66(18): 3191-3199, doi: 10.1016/S0016-7037(02)00918-3.

Rowe, E.C., Schilling, J.G., 1979. Fluorine in Iceland and Reykjanes Ridge basalts. Nature, 279(5708): 33-37, doi: 10.1038/279033a0.

Ryan, W.B.F. et al., 2009. Global Multi-Resolution Topography synthesis. Geochemistry Geophysics Geosystems, 10(3), doi: 10.1029/2008gc002332.

Saal, A.E., Hauri, E.H., Langmuir, C.H., Perfit, M.R., 2002. Vapour undersaturation in primitive mid-ocean-ridge basalt and the volatile content of Earth's upper mantle. Nature, 419: 451-455.

Salters, V.J.M., Stracke, A., 2004. Composition of the depleted mantle. Geochemistry Geophysics Geosystems, 5(5), doi: 10.1029/2003GC000597.

Schilling, J.-G., Kingsley, R.H., in prep. Highly siderophile element (HSE) abundances in basalts from the Reykjanes Ridge and the Iceland South West Rift Zone from 50°N to 65°N: Implications on HSE mantle source heterogeneities.

Schilling, J.-G., Kingsley, R.H., Fontignie, D., Poreda, R.J., Xue, S., 1999. Dispersion of the Jan Mayen and Iceland mantle plumes in the Arctic: A He-Pb-Nd-Sr isotope tracer study of basalts from the Kolbeinsey, Mohns, and Knipovich Ridges. Journal of Geophysical Research, 104(B5): 10543-10569.

Schilling, J.G., 1973. Iceland Mantle Plume: Geochemical Study of Reykjanes Ridge. Nature, 242(5400): 565-571, doi: 10.1038/242565a0.

Schilling, J.G., Bergeron, M.B., Evans, R., Smith, J.V., 1980. Halogens in the Mantle Beneath the North Atlantic [and Discussion]. Philosophical Transactions of the Royal Society of London. Series A, Mathematical and Physical Sciences, 297(1431): 147-178.

Schilling, J.G., Sigurdsson, H., 1979. Thermal Minima Along the Axis of the Mid-Atlantic Ridge. Nature, 282(5737): 370-375, doi: 10.1038/282370a0.

Schilling, J.G. et al., 1983. Petrologic and geochemical variations along the Mid-Atlantic Ridge from 29°N to 73°N. American Journal of Science, 283(6): 510-586, doi: 10.2475/ajs.283.6.510.

Sigurdsson, H., 1981. First-Order Major Element Variation in Basalt Glasses From the Mid-Atlantic Ridge: 29°N to 73°N. Journal of Geophysical Research, 86(B10): 9483-9502, doi: 10.1029/JB086iB10p09483.

Simons, K., Dixon, J.E., Schilling, J.-G., Kingsley, R.H., Poreda, R., 2002. Volatiles in basaltic glasses from the Easter-Salas y Gomez Seamount Chain and Easter Microplate: Implications for geochemical cycling of volatile elements. Geochemistry Geophysics Geosystems, 3(7), doi: 10.1029/2001GC000173.

Stagno, V., Ojwang, D.O., McCammon, C.A., Frost, D.J., 2013. The oxidation state of the mantle and the extraction of carbon from Earth's interior. Nature, 493(7430): 84-8, doi: 10.1038/nature11679.

Sun, S.-S., Tatsumoto, M., Schilling, J.-G., 1975. Mantle Plume Mixing Along the Reykjanes Ridge Axis: Lead Isotopic Evidence. Science, 190(4210): 143-147.

Unni, C.K., Schilling, J.G., 1978. Cl and Br degassing by volcanism along the Reykjanes Ridge and Iceland. Nature, 272(5648): 19-23, doi: 10.1038/272019a0.

Wallace, P., Carmichael, I.S.E., 1992. Sulfur in Basaltic Magmas. Geochimica Et Cosmochimica Acta, 56(5): 1863-1874, doi: 10.1016/0016-7037(92)90316-B.

Wang, Z., Becker, H., 2013. Ratios of S, Se and Te in the silicate Earth require a volatile-rich late veneer. Nature, 499(7458): 328-331, doi: 10.1038/nature12285

White, R.S., McKenzie, D., 1995. Mantle plumes and flood basalts. Journal of Geophysical Research, 100(B9): 17543-17585.

Wood, B.J., Bryndzia, L.T., Johnson, K.E., 1990. Mantle oxidation-state and its relationship to tectonic environment and fluid speciation. Science, 248: 337-345.

Wood, B.J., Pawley, A., Frost, D.R., 1996. Water and carbon in the Earth's mantle. Philosophical Transactions of the Royal Society a-Mathematical Physical and Engineering Sciences, 354(1711): 1495-1511, doi: 10.1098/Rsta.1996.0060.

Yi, W. et al., 2000. Cadmium, indium, tin, tellurium, and sulfur in oceanic basalts: Implications for chalcophile element fractionation in the Earth. Journal of Geophysical Research, 105(B8): 18927-18948, doi: 10.1029/2000jb900152.

Table 1. S, Se and Te contents of basalts from the Reykjanes Ridge and SW Iceland Rift Zone.

Sample Name	IGSN	Material	Latitude (°N)	Longitude (°W)	Elevation (km)	S (ppm)	Se (ppb)	Te (ppb)	Cu (ppm) [1]	$(La/Sm)_N$ [1]	Vol.% Vesicles [2]
IC-117g	URI00000Z	Glass	65.00	19.58		715	114	14.5	136	0.185	
IC-17	URI00001A	Whole Rock	64.73	20.78	0.400	97	90.5	0.254	144	1.15	17.1
IC-15	URI00001B	Whole Rock	64.68	17.68	0.300	63			146	1.10	5.6
IC-19	URI00001C	Whole Rock	64.66	19.16	0.600		44.7	0.479	118	0.978	7.1
HS-785g	URI00001D	Glass	64.45	21.08	0.500		201	8.82			
IC-3g	URI00001E	Glass	64.33	21.00	0.085	480	109	7.31			
IC-3	URI00001F	Whole Rock	64.33	21.00	0.085	224	105	7.46			
IC-13g	URI00001G	Glass	64.33	21.00	0.150	510	152	7.24			
IC-13	URI00001H	Whole Rock	64.33	21.00	0.150	159	73.0	7.09			
IC-12	URI00001I	Whole Rock	64.28	21.11	0.155	54	88.2	0.582			19.9
IC-9	URI00001J	Whole Rock	64.28	21.11	0.146	21	67.9	0.656	136	1.13	6.2
IC-11	URI00001K	Whole Rock	64.28	20.44	0.150	20	57.5	0.495	118	1.10	13.8
IC-10	URI00001L	Whole Rock	64.23	18.99	0.147	6	67.9	0.347	105	1.06	8.5
IC-36	URI00001M	Whole Rock	64.10	21.90	0.250	11	80.9	0.864	144	1.08	17.4
IC-43	URI00001N	Whole Rock	63.98	21.97	0.300	48	103	0.404			28.0
IC-62	URI00001O	Whole Rock	63.98	22.57	0.140	97	115	0.428	127	1.17	
IC-55	URI00001P	Whole Rock	63.97	21.74	0.030		14.3	0.311	124	0.897	21.8
IC-56	URI00001Q	Whole Rock	63.97	21.74	0.080		38.5	0.414	137	1.05	
IC-47	URI00001R	Whole Rock	63.95	22.20	0.460	15	90.3	0.661	128	1.25	1.2
IC-6g	URI00001S	Glass	63.91	22.54	0.100	640	177	5.89			
IC-58	URI00001T	Whole Rock	63.90	22.05	0.070	82	113	0.579	135	1.25	
HS-529	URI00001U	Whole Rock	63.86	22.43	0.080	79	150	1.86	169	1.25	26.4
HS-524	URI00001V	Whole Rock	63.85	22.70	0.010	97	138	1.24	142	1.14	9.1
TR101 15D-8g	URI900555	Glass	63.57	23.70	-0.083	1790	224	5.66	132	1.01	
TR101 15D-5	URI900554	Whole Rock	63.57	23.70	-0.083	632	205	4.56			20.8
TR101 19D-1	URI900561	Whole Rock	63.47	23.80	-0.105	680	233	4.14	137	1.05	28.8
TR101 16D-4	URI900558	Whole Rock	63.47	23.87	-0.060	604	133	5.83	119	0.899	18.2
TR101 17D-1	URI900559	Whole Rock	63.46	23.85	-0.040	150	127	0.816	103	0.939	15.4
TR101 18D-1	URI900560	Whole Rock	63.46	23.85	-0.043	663	147	3.41	131	1.05	17.1
TR101 10D-1	URI900536	Whole Rock	63.28	24.24	-0.162	577	225	4.64	146	1.03	
TR101 11D-2g	URI900539	Glass	63.27	24.20	-0.075	548	170	1.31	131	1.06	
TR101 11D-2	URI00000W	Whole Rock	63.27	24.20	-0.075	305	137	1.11			3.5
TR101 12D-6g	URI900544	Glass	63.22	24.27	-0.258		244	4.12	131	1.06	24.6
TR101 12D-7g	URI900545	Glass	63.22	24.27	-0.258	1403	202	3.68	142	1.06	11.8
TR101 14D-9g	URI900551	Glass	63.19	24.46	-0.345	1488	293	9.31	120	0.975	
TR101 07D-5g	URI900535	Glass	63.07	24.50	-0.315	1258	284	9.27	131	0.828	
TR101 07D-5	URI00000V	Whole Rock	63.07	24.50	-0.315	622	158	6.20			16.7
TR101 06D-9g	URI900532	Glass	62.99	24.69	-0.400	1125	240	9.24	132	1.06	28.6
TR101 05D-4g	URI900527	Glass	62.90	24.88	-0.505	1213	239	7.50	133	1.14	13.0
TR101 05D-2	URI900526	Whole Rock	62.90	24.88	-0.505	473	173	4.26			13.0
TR101 03D-1g	URI900522	Glass	62.79	25.16	-0.620	1320	234	11.1	132	1.03	
TR101 03D-1	URI00000U	Whole Rock	62.79	25.16	-0.620	770	182	11.6			22.5
TR101 03D-5	URI900525	Whole Rock	62.79	25.16	-0.620	538	200	11.1			3.6
TR101 35D-3g	URI900602	Glass	62.70	25.21	-0.580	1458	315	11.8	109	0.935	10.5
TR101 02D-1g	URI900519	Glass	62.62	25.43	-0.632	1313	250	9.07	119	0.954	17.4
TR101 01D-2g	URI900516	Glass	62.59	25.45	-0.617	1288	217	14.1	119	0.951	10.9
TR101 22D-1g	URI900562	Glass	62.37	25.84	-0.715	1318	264	10.6	105	0.712	24.6
TR101 22D-2g	URI900563	Glass	62.37	25.84	-0.715	1308	231	8.83			
TR101 23D-1g	URI900566	Glass	62.35	25.78	-0.657	1150	229	8.93	112	0.857	6.8
EN025 09D-1g	URI900494	Glass	62.31	25.93	-0.750	1178	237	9.02	111	1.12	
TR101 34D-6g	URI900598	Glass	62.26	26.14	-0.500	1113	149	9.21	114	0.846	26.2
TR101 25D-10g	URI900573	Glass	62.11	26.36	-0.686	1455	328	10.0	97.9	0.608	
TR101 25D-1	URI900572	Whole Rock	62.11	26.36	-0.686	877	159	16.4			12.5
TR101 24D-1g	URI900568	Glass	62.08	26.29	-0.682	1215	216	8.09	104	0.526	
TR101 24D-6	URI900570	Whole Rock	62.08	26.29	-0.682	595	162	11.1			6.8
EN025 08D-4g	URI900493	Glass	61.98	26.54	-0.730	1215	172	6.56	104	0.900	
EN025 08D-4	URI00000Q	Whole Rock	61.98	26.54	-0.730		169	8.55			
TR101 27D-1g	URI900574	Glass	61.73	26.88	-0.599	1045	97.1	9.70	113	0.493	6.7
TR101 27D-7g	URI900578	Glass	61.73	26.88	-0.599	1053	244	9.32	114	0.543	
TR101 27D-11	URI900579	Whole Rock	61.73	26.88	-0.599	656	133	11.3			4.3
EN025 06D-1g	URI900485	Glass	61.60	27.07	-0.760	1260	250	6.98	110	0.657	
EN025 06D-2g	URI900486	Glass	61.60	27.07	-0.760	1275	215	6.40			
EN025 06D-3g	URI900487	Glass	61.60	27.07	-0.760	1263	244	6.44	101	0.705	
EN025 06D-3	URI00000P	Whole Rock	61.60	27.07	-0.076	900	175	11.4			
EN025 06D-4g	URI900488	Glass	61.60	27.07	-0.760	1318	175	9.30			
EN025 06D-5g	URI900489	Glass	61.60	27.07	-0.760	1288	265	9.42			
TR101 29D-4g	URI900583	Glass	61.10	27.88	-0.810	1280	225	9.33	107	0.400	
TR101 29D-5	URI900584	Whole Rock	61.10	27.88	-0.081	1582	230	12.0			8.7
TR101 30D-2g	URI900585	Glass	61.09	27.90	-0.792	1258	257	9.24	108	0.304	
TR101 30D-10g	URI900587	Glass	61.09	27.90	-0.792	1230	272	10.7	112	0.312	
TR101 30D-10	URI00000X	Whole Rock	61.09	27.90	-0.792	756	156	16.2			13.5
TR101 31D-2g	URI900589	Glass	60.73	28.42	-0.710	1308	255	9.66	111	0.326	
TR101 31D-8g	URI900592	Glass	60.73	28.42	-0.710	1293	214	8.98			12.0
TR101 33D-6g	URI900595	Glass	60.45	28.88	-0.922	1265	226	14.3	119	0.155	7.8
TR041 D20-3g	URI900502	Glass	60.03	29.38	-0.948	1393	248	8.25	112	0.273	5.0
TR041 D22-4g	URI900504	Glass	60.02	29.48	-0.978	1305	214	9.35	116	0.273	
TR041 D19-1g	URI900501	Glass	59.99	29.43	-0.950	1320	164	12.5	107	0.252	
TR041 D19-1	URI00000S	Whole Rock	59.99	29.43	-0.950	714	166	16.2			6.0
TR041 D38-2g	URI900505	Glass	59.99	29.51	-0.925	1338	231	10.5	98.4	0.445	8.8
TR041 D18-2g	URI900500	Glass	59.99	29.53	-1.040	1418	249	12.2	110	0.238	
GLJ 10g	URI900499	Glass	58.87	30.95	-1.383	1445	224	7.97	91.2	0.275	
GLJ 10	URI00000R	Whole Rock	58.87	30.95	-1.383	927	144	7.90			3.0

EN025 05D-2g	URI900482	Glass	58.42	31.62	-1.457	1148	170	8.62			
EN025 05D-2	URI00000O	Whole Rock	58.42	31.62	-1.457	624	133	8.88			
EN025 05D-3g	URI900483	Glass	58.42	31.62	-1.457	1128	217	11.1	85.0	0.528	
EN025 05D-4g	URI900484	Glass	58.42	31.62	-1.457	1153	208	7.98			
TR100 26D-10	URI900513	Whole Rock	57.68	32.57	-1.380	803	167	6.32			1.7
EN025 04D-1g	URI900478	Glass	57.14	33.42	-2.160	1288	202	5.92	84.9	0.423	
EN025 04D-1	URI00000M	Whole Rock	57.14	33.42	-2.160	982	150	6.97			
EN025 04D-2g	URI900479	Glass	57.14	33.42	-2.160	1303	211	4.55			
EN025 04D-2	URI00000N	Whole Rock	57.14	33.42	-2.160	899	162	6.77			
EN025 04D-3g	URI900480	Glass	57.14	33.42	-2.160	1290	173	6.41			
EN025 03D-4g	URI900477	Glass	55.67	34.87	-1.975	1273	198	11.2	94.6	0.366	
EN025 02D-1g	URI900470	Glass	54.76	35.22	-2.075	1318	220	9.18			
EN025 02D-2g	URI900471	Glass	54.76	35.22	-2.075	1335	222	10.0			
EN025 02D-3g	URI900472	Glass	54.76	35.22	-2.075	1310	206	9.04			
EN025 02D-4g	URI900473	Glass	54.76	35.22	-2.075	1318	203	6.30	94.6	0.371	
TR100 23D-10g	URI900512	Glass	54.25	35.40	-0.880	1203	243	8.45	91.2	0.216	0.2
EN025 01D-1g	URI900469	Glass	53.41	35.24	-2.400	1413			74.8	0.373	
EN025 01D-1	URI900469	Whole Rock	53.41	35.24	-2.400	848	177	5.16			
GLJ 7g	URI900498	Glass	52.66	34.94	-3.239	1370	175	6.90	82.0	0.353	0.0
TR100 13D-10g	URI900510	Glass	52.48	31.57	-4.050	1205	100	1.81	67.8	0.595	
TR100 13D-10	URI00000T	Whole Rock	52.48	31.57	-4.050	877	105	2.07			0.6
TR100 12D-7g	URI900508	Glass	52.33	31.52	-2.400	1270	84.6	1.09			
TR138 11D-1g	URI900610	Glass	52.01	29.95	-3.800	1228	121	2.26	63.3	0.520	0.7
TR138 09D-2g	URI900608	Glass	51.56	29.92	-3.710	1273	115	2.44	54.5	0.456	0.9
TR138 08D-1g	URI900606	Glass	51.28	30.02	-3.500	970	102	2.41	50.4	0.522	4.7
TR138 07D-1Ag	URI900603	Glass	50.46	29.42	-3.880	988	102	1.88	62.4	0.487	
TR138 07D1A	URI00000Y	Whole Rock	50.46	29.42	-3.880	793	79.0	2.43			1.0
Bulk Earth [3]						250	75	12.0	30	1.00	
CI Chondrites [3]						54000	21000	2330	120	1.00	

[1] Data preiously reported by Kelley et al. (2013) or Schilling et al. 1983
[2] Data previously reported by Schilling et al. (1983) or Moore & Schilling (1973).
[3] Values from McDonough & Sun (1995).

Figure 1

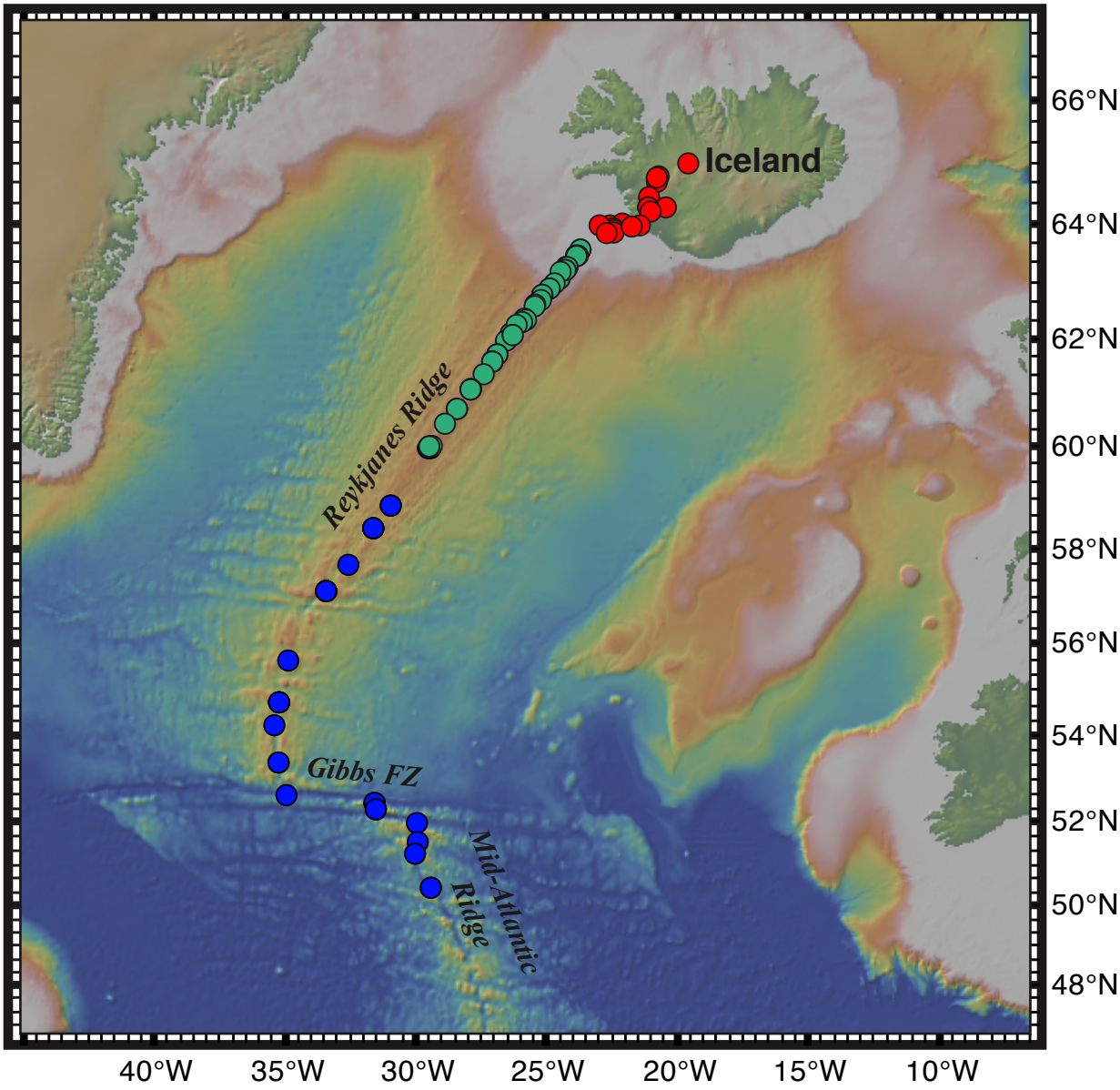
Iceland
Reykjanes Ridge
Gibbs FZ
Mid-Atlantic Ridge
66°N
64°N
62°N
60°N
58°N
56°N
54°N
52°N
50°N
48°N
40°W
35°W
30°W
25°W
20°W
15°W
10°W

Figure 2

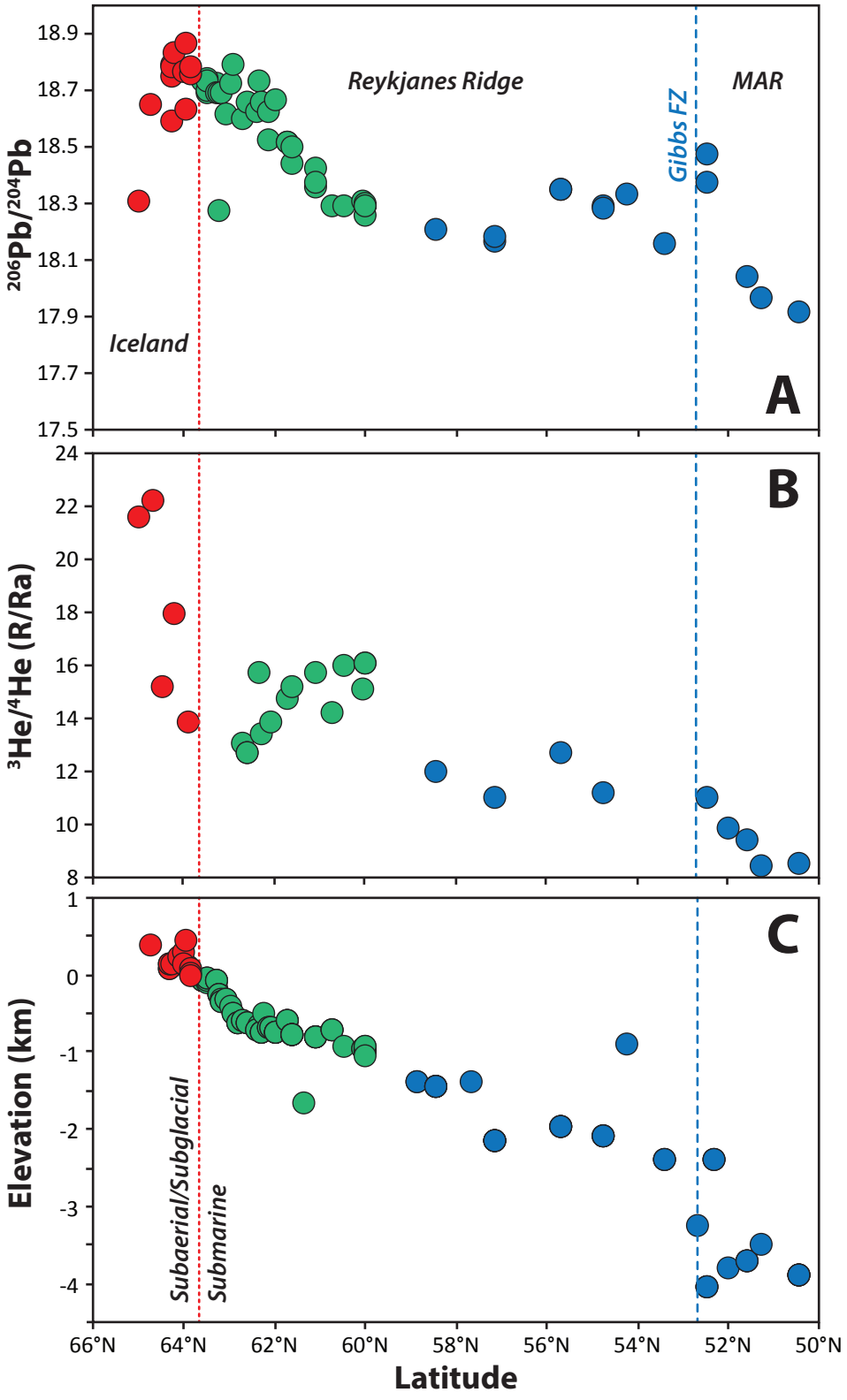
Reykjanes Ridge
MAR
Gibbs FZ
Iceland
A
B
C
Subaerial/Subglacial
Submarine
$^{206}Pb/^{204}Pb$
$^{3}He/^{4}He$ (R/Ra)
Elevation (km)
Latitude
18.9
18.7
18.5
18.3
18.1
17.9
17.7
17.5
24
22
20
18
16
14
12
10
8
1
0
-1
-2
-3
-4
66°N
64°N
62°N
60°N
58°N
56°N
54°N
52°N
50°N

Figure 3

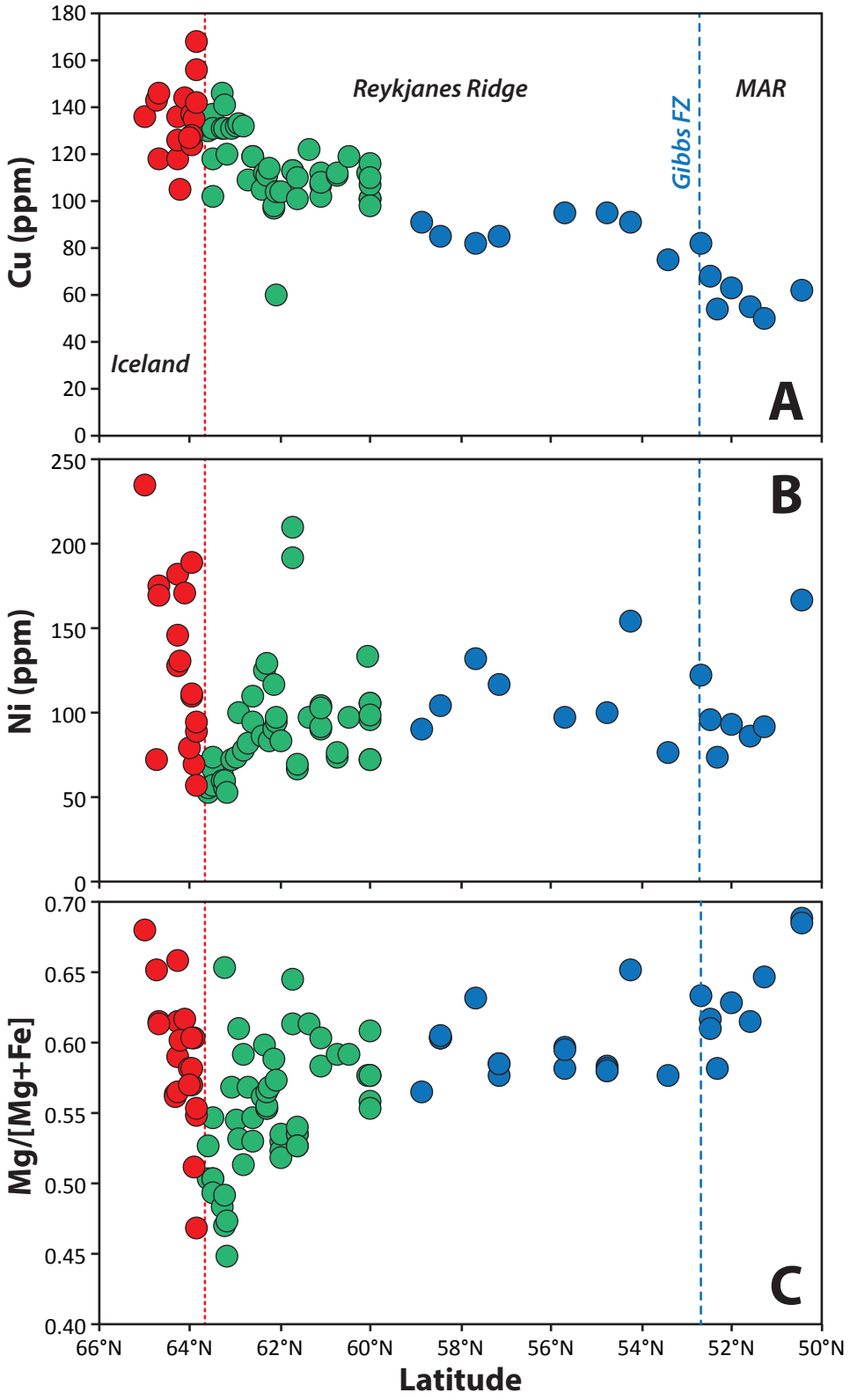
Cu (ppm)
Reykjanes Ridge
Gibbs FZ
MAR
Iceland
A
Ni (ppm)
B
Mg/[Mg+Fe]
C
Latitude
66°N
64°N
62°N
60°N
58°N
56°N
54°N
52°N
50°N

Figure 4

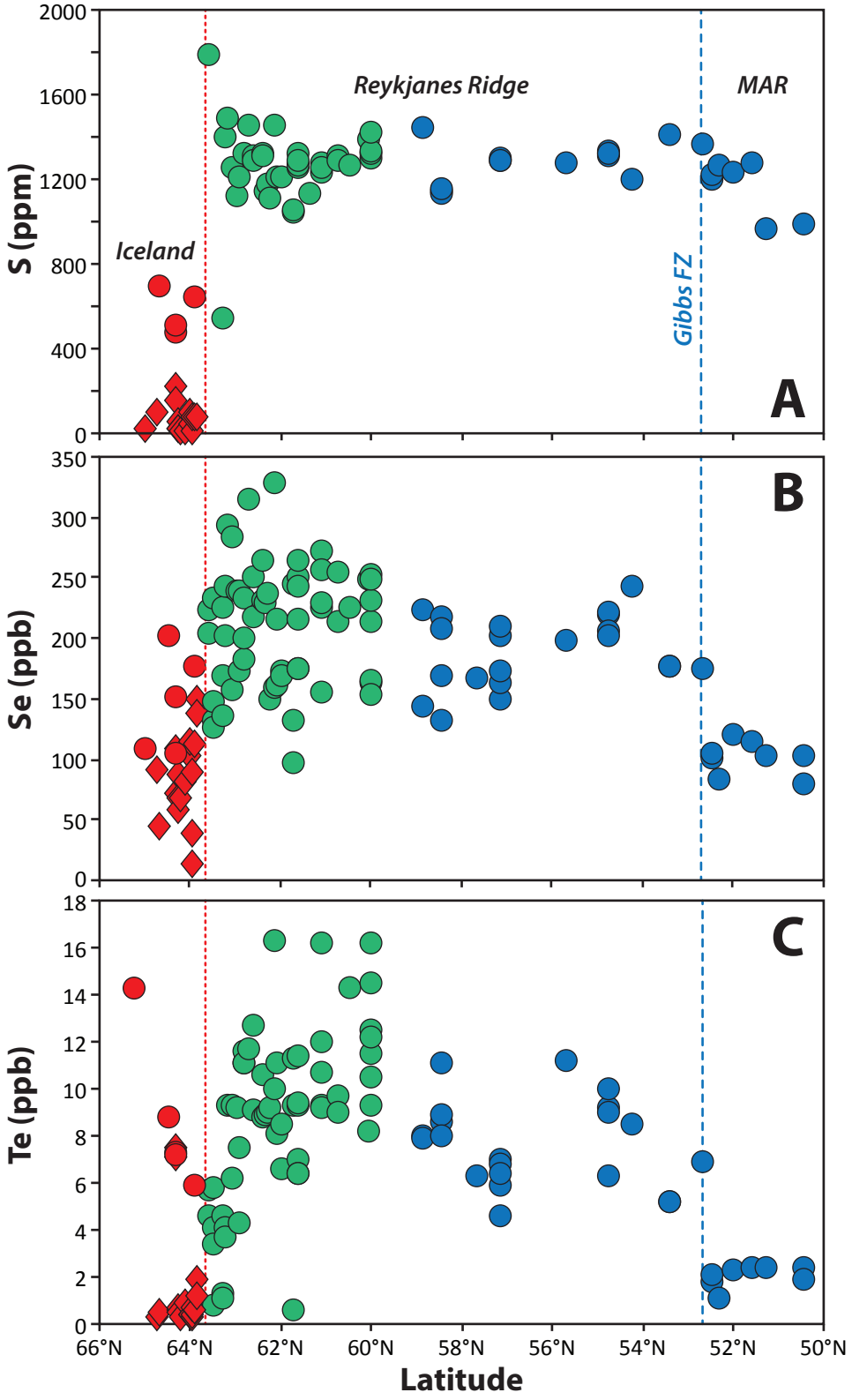
S (ppm)
2000
1600
1200
800
400
0
Reykjanes Ridge
MAR
Iceland
Gibbs FZ
A
Se (ppb)
350
300
250
200
150
100
50
0
B
Te (ppb)
18
16
14
12
10
8
6
4
2
0
C
66°N
64°N
62°N
60°N
58°N
56°N
54°N
52°N
50°N
Latitude

Figure 5

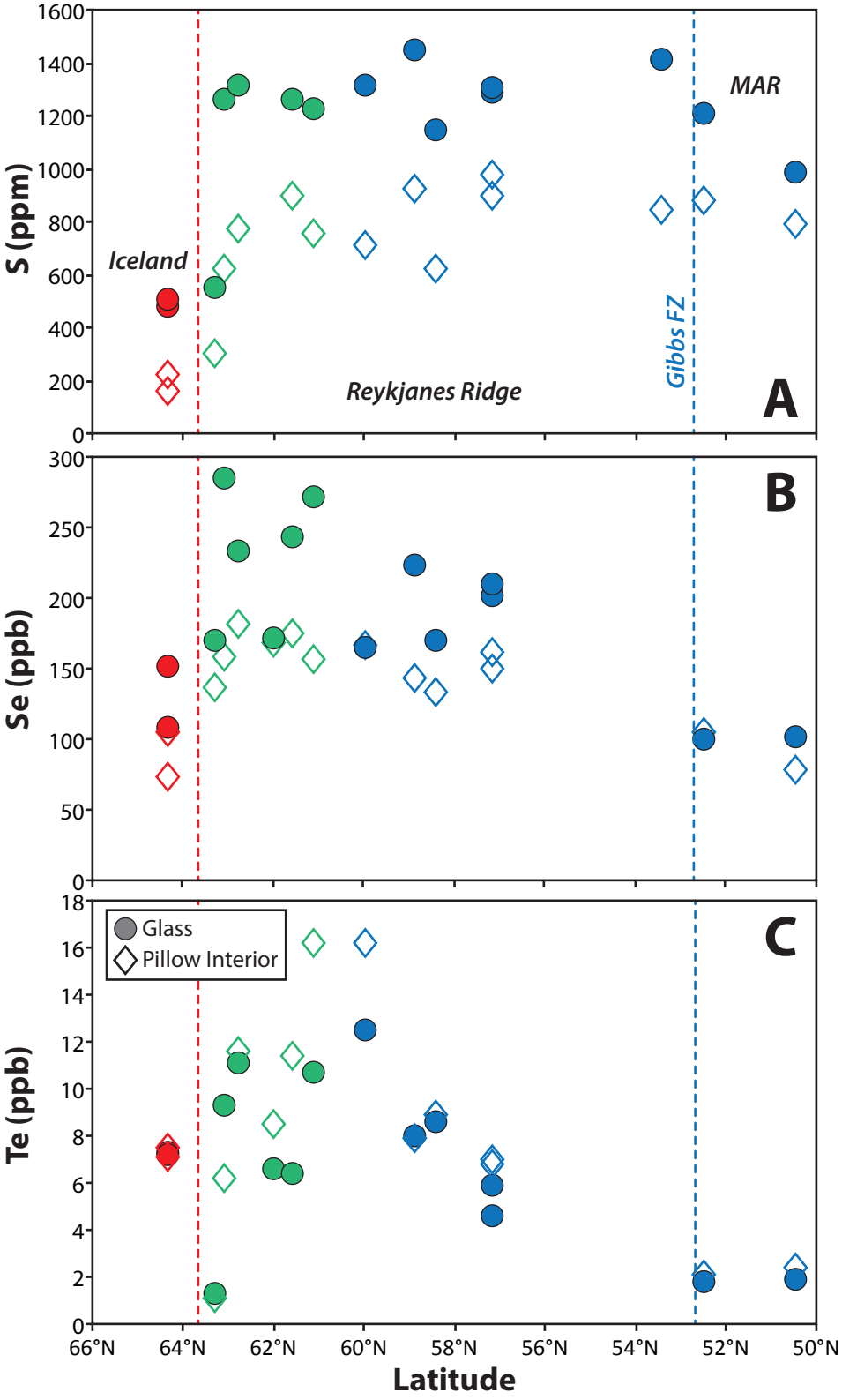
S (ppm)
Se (ppb)
Te (ppb)
Iceland
Reykjanes Ridge
Gibbs FZ
MAR
A
B
C
Glass
Pillow Interior
66°N
64°N
62°N
60°N
58°N
56°N
54°N
52°N
50°N
Latitude

Figure 6

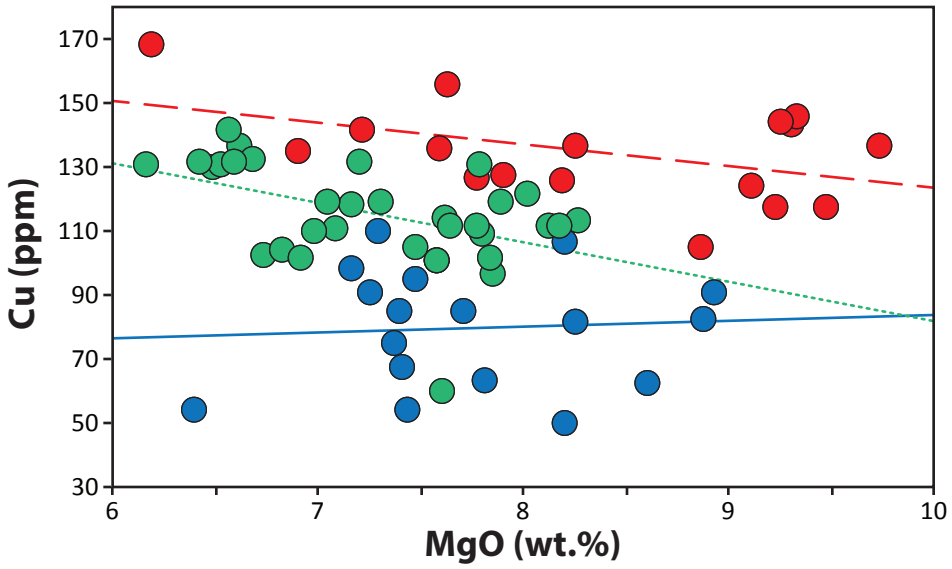

Figure 7

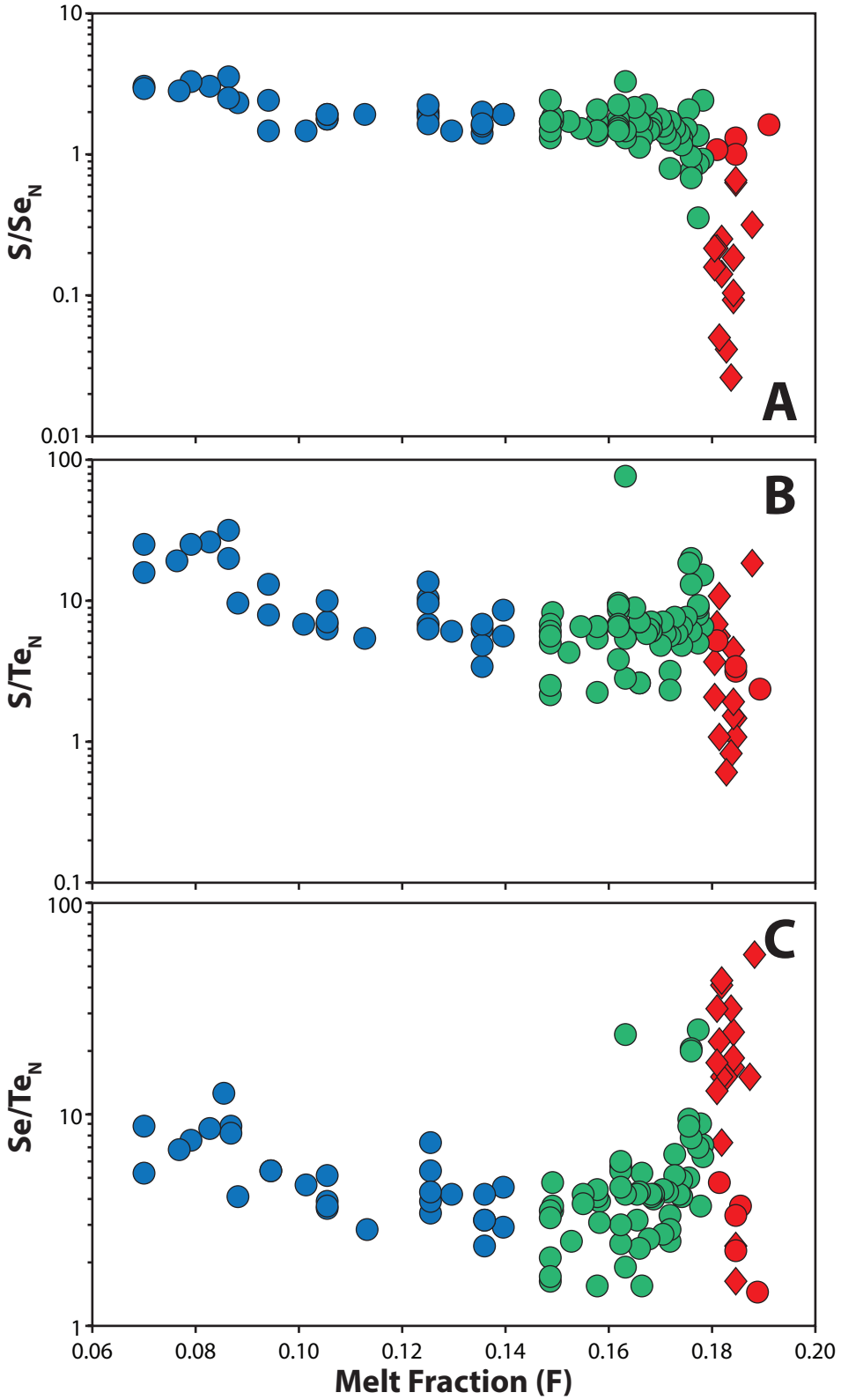
10
1
0.1
0.01
S/Se$_N$
A
100
10
1
0.1
S/Te$_N$
B
100
10
1
Se/Te$_N$
C
0.06
0.08
0.10
0.12
0.14
0.16
0.18
0.20
Melt Fraction (F)

Figure 8

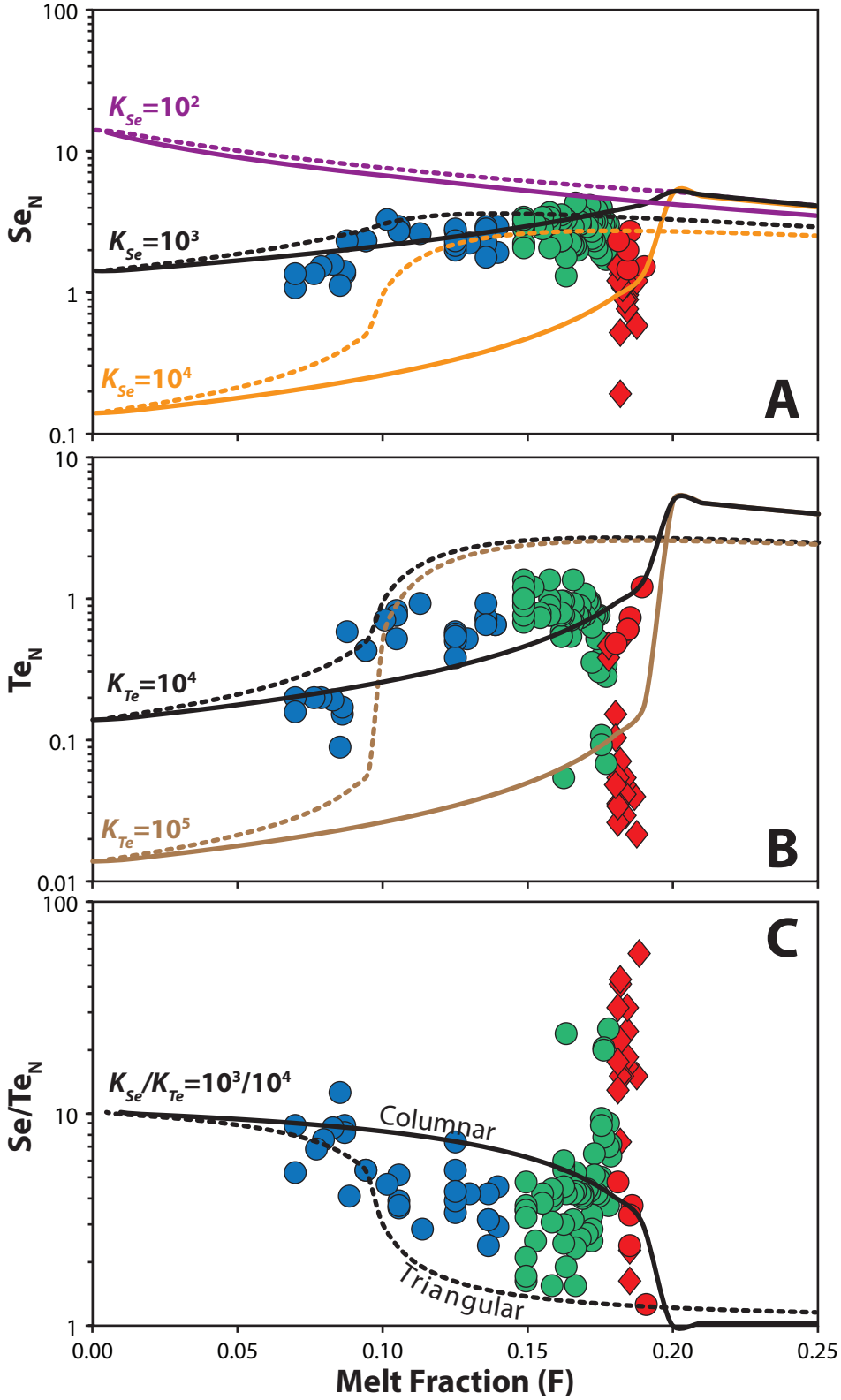
100
10
1
0.1
Se_N
$K_{Se}=10^2$
$K_{Se}=10^3$
$K_{Se}=10^4$
A
10
1
0.1
0.01
Te_N
$K_{Te}=10^4$
$K_{Te}=10^5$
B
100
10
1
Se/Te_N
$K_{Se}/K_{Te}=10^3/10^4$
Columnar
Triangular
C
0.00
0.05
0.10
0.15
0.20
0.25
Melt Fraction (F)

Figure 9

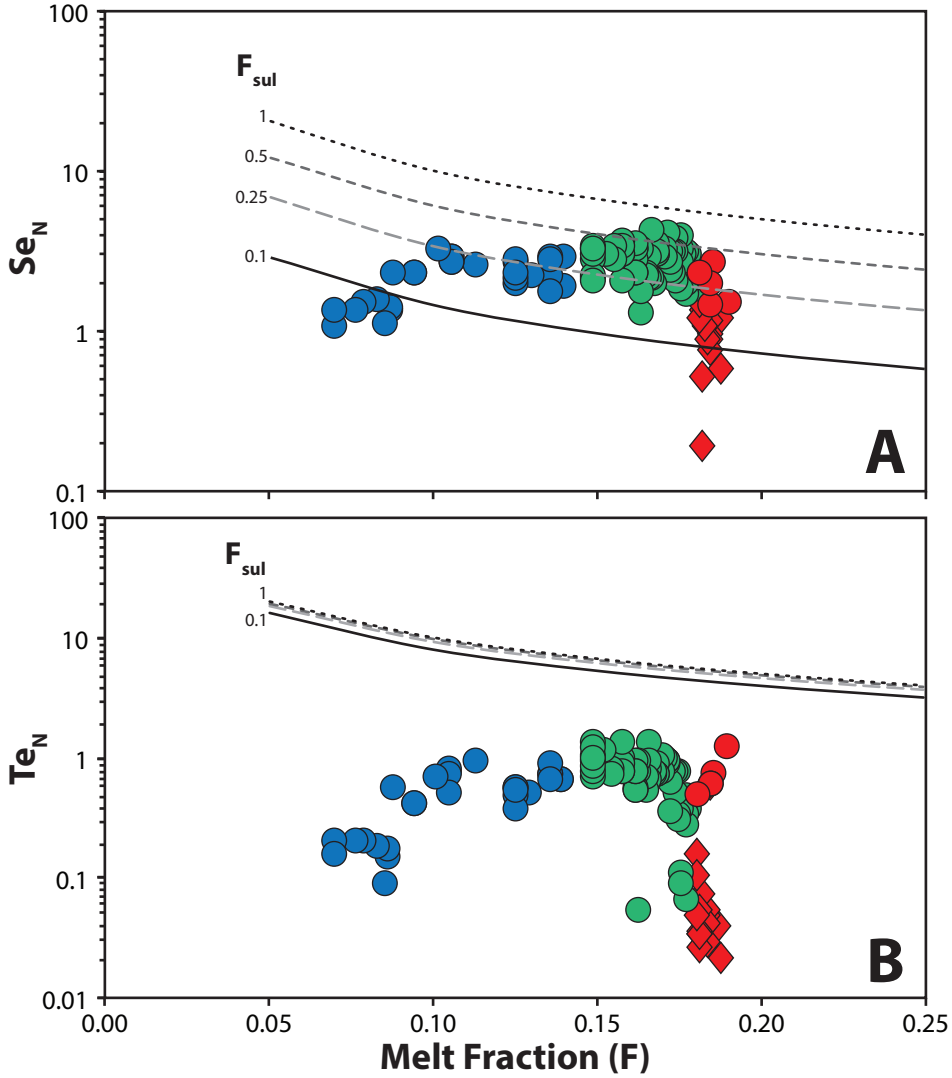
100
10
1
0.1
Se_N
F_{sul}
1
0.5
0.25
0.1
A
100
10
1
0.1
0.01
Te_N
F_{sul}
1
0.1
B
0.00
0.05
0.10
0.15
0.20
0.25
Melt Fraction (F)

Supplementary Information to Accompany
"Se, Te and S variations in basalts along the Reykjanes Ridge and extension over Iceland, from 50°N to 65°N"

Sulfide/Silicate Melt Partitioning of Se and Te

Compared to the comprehensive study of Se and Te sulfide/silicate melt partitioning measurements and study of *Brenan* [in revision], the measurements in MORB of coexisting sulfide globule/silicate glass partition coefficients, $K^{\text{globule sulfide /silicate melt}}$ reported by *Patten et al.* [2013] appear lower by up to a factor of 3. They average 4478 ± 1146 for Te and 345±37 for Se [*Patten et al.*, 2013; though an earlier 1770 value for Se has also been reported by *Peach et al.*, 1990]. The lower $K^{\text{sulfide /silicate melt}}$ values of *Patten et al.* [2013] may be an artifact of how they were determined. In this regard, *Brenan* [in revision] points out that *Patten et al.* [2013] determined empirical partition coefficients using glass compositions from similar samples reported by *Jenner and O'Neill* [2012] and *Yi et al.* [2000] for Se and Te, respectively. At comparable MgO content, Se partition coefficients from *Patten et al.* [2013] are about a factor of 3 lower than those reported by *Brenan* [in revision]. This is consistent with our observation that the Se contents for N-MORB reported by *Jenner and O'Neill* [2012] appear to be up to a factor 3 too high compared with our own values (see Section 4 and the below discussion).

Assessment of Inter-Laboratory Biases in Se Concentrations

To evaluate the potential for inter-laboratory biases that may explain the systematic offset between the Se data of *Jenner and O'Neill* [2012] and those of the present study, we compared data for Se in certified reference materials in the papers reporting methodologies for both studies [*Forrest et al.*, 2009; *Jenner et al.*, 2009]. The two studies contain no glasses in common, so it is impossible to directly compare the results of the two methods. Important to note is that the methods of *Jenner and O'Neill* [2012] and *Jenner et al.* [2009] are LA-ICP-MS analyses of glass, whereas the analyses of our study were performed on dissolved aliquots of bulk glass. The differences in sampling methods, however, are not sufficient to explain a factor of 2-3 difference in Se concentration. If the bulk glass contained micro-globules or micro-phenocrysts of sulfides containing Se, one would expect the bulk glass Se concentrations to be higher.

Rather, we suggest that there are inherent differences in the calibrations of the two methods that result in a systematic difference in Se concentration. Figure S1 shows the recommended Se concentrations for reference materials analyzed by *Jenner et al.* [2009] and *Forrest et al.* [2009], plotted against the concentrations determined using the calibrations of both methods. For the samples determined by *Forrest et al.* [2009], four out of five basalts fall close to 1:1 agreement with recommended values for Se (the sole outlier, W-2, is attributed to heterogeneity due to powder settling). The reference glasses reported by *Jenner et al.* [2009], however, fall to systematically higher Se concentrations relative to the recommended values reported by *Jochum et al.* [2006], by about a factor of two, save for one outlier (KL2-G) that is not discussed. Based on this assessment, we propose that there is a significant inter-laboratory bias between the data of *Jenner and O'Neill* [2012] and the data we present here, with the former being a factor of ~2-3 higher largely as a result of the calibration offset shown in Figure S1.

Figure Captions

Figure S1. Plot of recommended Se concentrations vs. analyzed Se concentrations in powdered and glass reference materials from the studies of *Jenner et al.* [2009] (diamonds; LA-ICP-MS) and *Forrest et al.* [2009] (circles; HG-ICP-MS). Recommended values for Se in the reference materials shown are from the GeoReM database and reported by *Jochum et al.* [2006]. The solid gray line is 1:1 correspondence, and the dotted line is 2:1 bias.

References

Brenan, J. M. (in revision), Se-Te fractionation by sulfide–silicate melt partitioning: Implications for the composition of mantle-derived magmas and their melting residues, *Earth Planet. Sci. Lett.*

Forrest, A., R. Kingsley, and J.-G. Schilling (2009), Determination of Selenium and Tellurium in Basalt Rock Reference Materials by Isotope Dilution Hydride Generation-Inductively Coupled Plasma-Mass Spectrometry (ID-HG-ICP-MS), *Geostandards and Geoanalytical Research*, *33*(2), 261-269, doi:10.1111/j.1751-908X.2009.00841.x.

Jenner, F. E., P. Holden, J. A. Mavrogenes, H. S. C. O'Neill, and C. Allen (2009), Determination of Selenium Concentrations in NIST SRM 610, 612, 614 and

Geological Glass Reference Materials Using the Electron Probe, LA-ICP-MS and SHRIMP II, *Geostandards and Geoanalytical Research*, *33*(3), 309-317, doi:10.1111/j.1751-908X.2009.00024.x.

Jenner, F. E., and H. S. C. O'Neill (2012), Analysis of 60 elements in 616 ocean floor basaltic glasses, *Geochem. Geophys. Geosys.*, *13*, doi:10.1029/2011gc004009.

Jochum, K. P., B. Stoll, K. Herwig, M. Willbold, A. W. Hofmann, M. Amini, S. Aarburg, W. Abouchami, E. Hellebrand, B. Mocek, I. Raczek, A. Stracke, O. Alard, C. Bouman, S. Becker, M. Dücking, H. Brätz, R. Klemd, D. de Bruin, D. Canil, D. Cornell, C.-J. de Hoog, C. Dalpé, L. V. Danyushevsky, A. Eisenhauer, Y. Gao, J. E. Snow, N. Groschopf, D. Günther, C. Latkoczky, M. Guillong, E. H. Hauri, H. E. Höfer, Y. Lahaye, K. Horz, D. E. Jacob, S. A. Kasemann, A. J. R. Kent, T. Ludwig, T. Zack, P. R. D. Mason, A. Meixner, M. Rosner, K. Misawa, B. P. Nash, J. Pfänder, W. R. Premo, W. D. Sun, M. Tiepolo, R. Vannucci, T. Vennemann, D. Wayne, and J. D. Woodhead (2006), MPI-DING reference glasses for in situ microanalysis: New reference values for element concentrations and isotope ratios, *Geochem. Geophys. Geosys.*, *7*(2), Q02008, doi:10.1029/2005GC001060.

Patten, C., S. J. Barnes, E. A. Mathez, and F. E. Jenner (2013), Partition coefficients of chalcophile elements between sulfide and silicate melts and the early crystallization history of sulfide liquid: LA-ICP-MS analysis of MORB sulfide droplets, *Chem. Geol.*, *358*, 170-188, doi:10.1016/J.Chemgeo.2013.08.040.

Peach, C. L., E. A. Mathez, and R. R. Keays (1990), Sulfide Melt-Silicate Melt Distribution Coefficients for Noble-Metals and Other Chalcophile Elements as Deduced from MORB - Implications for Partial Melting, *Geochim. Cosmochim. Acta*, *54*(12), 3379-3389, doi:10.1016/0016-7037(90)90292-S.

Yi, W., A. N. Halliday, J. C. Alt, D.-C. Lee, M. Rehkämper, M. O. Garcia, C. H. Langmuir, and Y. Su (2000), Cadmium, indium, tin, tellurium, and sulfur in oceanic basalts: Implications for chalcophile element fractionation in the Earth, *J. Geophys. Res.*, *105*(B8), 18927-18948, doi:10.1029/2000jb900152.

Figure S1

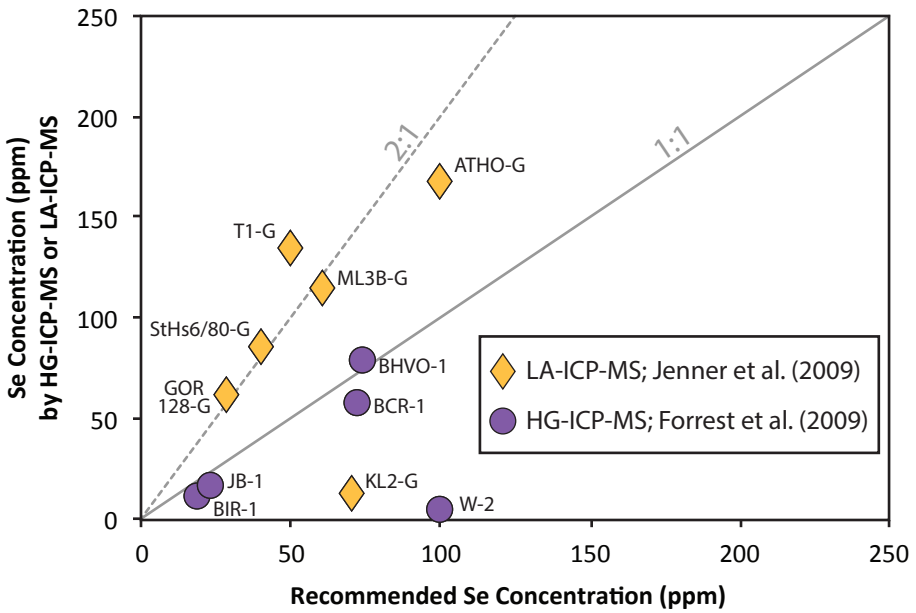

View publication stats